Characteristics of disordered Calcium aluminosilicates as supplementary cementitious materials

Master's Project
Chemistry Civil Engineer
Aalborg University
2. June 2025

Front page picture:[1]

Resume:
Hovedformålet med dette projekt, var at undersøge forskellen i karakteristika mellem uordnede CAS-materialer (Calcium Aluminosilicate) til anvendelse som SCM'er (Supplementary Cementitious Materials). Dette blev opnået ved at fokusere på implementeringen af kaolin og dolomit, og ved at undersøge termisk behandling af kaolin både uafhængigt og med tilsætning af $CaCO_3$. Ydermere blev mekanisk aktivering (MA) anvendt på kaolin og Ca-kaolin ved hjælp af en planetarisk kuglemølle med knusnings tiderne varierende fra 20 til 120 minutter. Artiklen analyserer virkningen af disse behandlinger på materialestruktur og reaktivitet, hvor XRD-data og målinger af bundet vand (vægt%) sammenlignes for at vurdere pozzolansk aktivitet. Resultaterne indikerer, at kaolin bidrager til høj reaktivitet, hvor MA viser sammenlignelige resultater med kalcinering for at forbedre tidlig reaktivitet. Tilsætningen af dolomit introducerer Mg, hvilket øger den tidlige reaktivitet betydeligt. Partikelstørrelsesanalyse afslørede, at MA af dolomit og $CaCO_3$ resulterer i større partikelstørrelser med øget knusning, hvilket korrelerer med forbedret reaktivitet. DSC blev anvendt til at sammenligne materialers reaktivitet med fokus på massetab mellem 400-500 °C som en indikator for CH-indhold. Resultaterne tyder på, at blandinger af kaolin og dolomit er lovende som SCM'er, især med MA, hvilket giver et omkostningseffektivt alternativ til højtemperatur kalcinerede materialer.

AALBORG UNIVERSITY
STUDENT REPORT

The Faculty of Engineering and Science
Fibigerstræde 16
9220 Aalborg Øst
Denmark
https://www.engineering.aau.dk

Title:

Characteristics of disordered Calcium aluminosilicates as supplementary cementitious materials

Project:

Masters Project

Project period:

September 2024 - June 2025

Participants:

Vigen Davtyan

Supervisors:

Shuai Nie
Yuanzheng Yue

Page number: 36
Appendix: 6
Finished: 02-06-2025

Abstract:

The main objective of this project was to investigate the difference in characteristics of disordered CAS materials for use as SCMs. This was achieved by focusing on the implementation of kaolin and dolomite, examining thermal treatment of kaolin treatment both independently and with the addition of $CaCO_3$. Furthermore, mechanical activation (MA) was applied to kaolin and Ca-kaolin using a planetary ball mill with milling times ranging from 20 to 120 minutes. The paper analyzes the impact of these treatments on material structure and reactivity, comparing XRD data and bound water (wt%) content measurements to assess pozzolanic activity. Results indicate that kaolin contributes to high reactivity, with MA showing comparable results to calcination for enhancing early reactivity. The addition of dolomite introduces Mg, significantly increasing early reactivity. Particle size analysis revealed that MA of dolomite and $CaCO_3$ results in larger particle sizes with increased milling time, correlating with improved reactivity. DSC was applied to compare material reactivity, focusing on mass loss between 400-500 °C as an indicator of CH content. The finding suggest that kaolin and dolomite blends hold promise as SCMs, particularly with MA, providing a cost-effective alternative to high-temperature calcined materials.

Preface

This project was developed by a chemical engineering students at Aalborg University.

Readers guide
The source references are numbered in order and are collected in a bibliography at the end of the report. The bibliography lists books with author, title, and publisher, while internet sources are listed with author, title, URL, and date visited. Figures, tables, and equations are numbered according to the respective chapter, for example, the first figure in chapter 3 has the number 3.1, the second figure number 3.2, and so on. Figure and table captions are found below and above their respective figures and tables respectively.

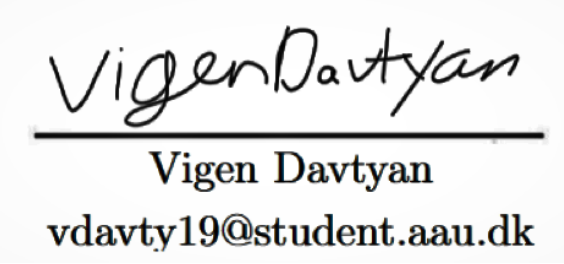

Vigen Davtyan
vdavty19@student.aau.dk

Abbreviation

CAS	- Calcium aluminosilicate
CH	- Calcium hydroxide
CMAS	- Calcium magnesium aluminosilicate
C-S-H	- calcium silicate hydrate
C2S	- Belite
C3S	- Alite
C3A	- Aluminate
C4AF	- Ferrite
FA	- Fly ash
MA	- Mechanochemical activation
SCM	- Supplementary Cementitious Materials
GBFS	- Granulated blast furnace slag
T_m	- Melting temperature
T_g	- Glass transition temperature

Contents

Introduction and problem analysis 1

Cement has throughout history shown to be an essential factor in construction, which through years of refining and optimization has led to the production of Portland cement. Cement mainly provides the binding agent in concrete with a wide range of applications, enabling many construction projects such as roads, buildings, bridges, and many more. First developed in the early 19th century and gaining widespread popularity during the industrial age, Portland cement is renowned for its strength, versatility and low cost. Different types of Portland cement has been developed for various applications, there is for example sulfate resistance cement, used near soil or groundwater, usually having higher sulfate contents[2]. Cement is used extensively in residential, commercial, and industrial construction projects worldwide, since the main components for Portland cement are calcium carbonate ($CaCO_3$), iron oxide (Fe_2O_3), alumina (Al_2O_3) and silica (SiO_2) which are abundant and easily accessible in raw earthy materials throughout the world, including the less fortunate countries[3].

The production process of Portland cement involves several stages, including the extracting and heating of raw materials like limestone ($CaCO_3$), which undergo calcination in rotary kilns reaching temperatures up to 1450°C. This process produces large quantities of CO_2, as after calcination the $CaCO_3$ loses CO_2 becoming CaO also known as lime which then reacts with other raw materials to form new minerals, called clinker. The whole process of producing cement contributes significantly to global greenhouse gas emissions where cement accounts for approximately 8% of global CO_2 emissions, here roughly 60% of the CO_2 comes from the chemical decomposition of raw materials, whereas the rest is due to the energy used[4]. To address this environmental challenge, the industry has turned to Supplementary Cementitious Materials (SCMs), such as fly ash (FA) and granulated blast furnace slag (GBFS) which are widely implemented, researched, and, have shown to be useful by partially replacing clinker in cement mixtures, reducing CO_2 emissions and improving concrete properties, where Giergiczny, Z. [5] even shows benefits, in the form of higher early strengths and greater durability of concretes when implementing 30- 40% fly ash. Giergiczny, Z. [5] also emphasizes the effect of mechanical activation by grinding, increasing clinker activity.

Even though the implementation of FA and GBFS is showing promise, the materials are not sustainable and can differ in quality depending on how they are obtained. These

materials can be used as SCMs since the chemical compositions are roughly the same as in Portland cement. In the same manner, materials such as calcium aluminosilicate glass (CAS-glass) and calcium-modified calcined clays present innovative alternatives to SCMs. CAS-glass, derived from industrial by-products or waste glass, and 1:1 clays composed of tetrahedral silica, and octehedral alumina sheets, can offer the potential for reduced-clinker cement production due to their chemical similarities to FA and GBFS. Here the 1:1 clay type kaolinite is well researched, showing greater promise than 2:1 clay types like illite and montmorillonite as a SCM [6].

However, integrating CAS-glass and calcium-modified calcined clay into Portland cement production is not without challenges. One significant issue is achieving the necessary reactivity and compatibility with existing cement systems to ensure consistent performance and durability. Additionally, the sourcing and processing of these materials must be economically viable and sustainable to support widespread adaptation. In this one study Borno, I. & Ashraf, W. [7] showed, that calcined kaolin, better known as metakaolin can be used as a SCM, if the natural kaolin clay source does not contain significant amounts of other clay materials such as montmorillonite, since this would lower the reactivity significantly.

By exploring these innovative SCMs, the cement industry can take significant steps toward more sustainable practices, potentially transforming cement production processes for a lower carbon future. Therefore the aim of this project is, to compare the structure of various disordered CAS materials, to test what effect the change in structure and components has on the pozzalinic reactivity.

These thoughts and concerns have led to the following problem delineation:

Which disordered structure has the best pozzolanic reactivity, and what effect will the incorporation of Ca/Mg have?. Furthermore What impact does calcination temperature have compared to mechanochemical activation for the clay materials. Lastly, is there an easy and reliable way to evaluate pozzolanic reactivity, through the use of DSC?

Theory 2

2.1 Clay

There are a lot of different types of clay, that consist of many different minerals which are found in earth's crust. It is said to have been created over millions of years, by the interactions of nature with the granite on the crust, forming mainly soda, quartz, and kaolinite [8].

Clay is a soft, plastic-like material due to its particle size, geometry, as well as its ability to absorb water, and becomes hard and non-plastic-like if dried or heated. Clay is composed of fine grained natural rocks or earthy materials and is mainly inorganic. When classifying clay, the upper limit for the size of the particles is not finite, but is mainly acknowledged to be below 5 µm. The minerals which make up clay can vary in their content of ions, such as iron, alkali metals, alkaline earth metals, and other cations. Clay minerals consist of both primary and secondary minerals. Primary minerals refer to those from metamorphic and igneous rocks that can break down through weathering or undergo structural changes. This process leads to the formation of secondary minerals, which often have a platy and flaky structure. The specific composition of these secondary minerals can significantly impact the chemical and physical properties of the clay.[9].

2.1.1 Clay classification

The type of clay most commonly referred to when we say "clay" is a layered structure made of aluminosilicate. Aluminosilicate consists of phyllosilicates, which are formed from layers of tetrahedral and octahedral arrangements. Phyllosilicates, being the most prevalent clay minerals, can be further categorized based on their composition and the number and arrangement of these layers. The main groups of clay minerals include layer silicates, chain silicates, sesquioxides, and other inorganic minerals.[10], as illustrated in Figure 2.1.

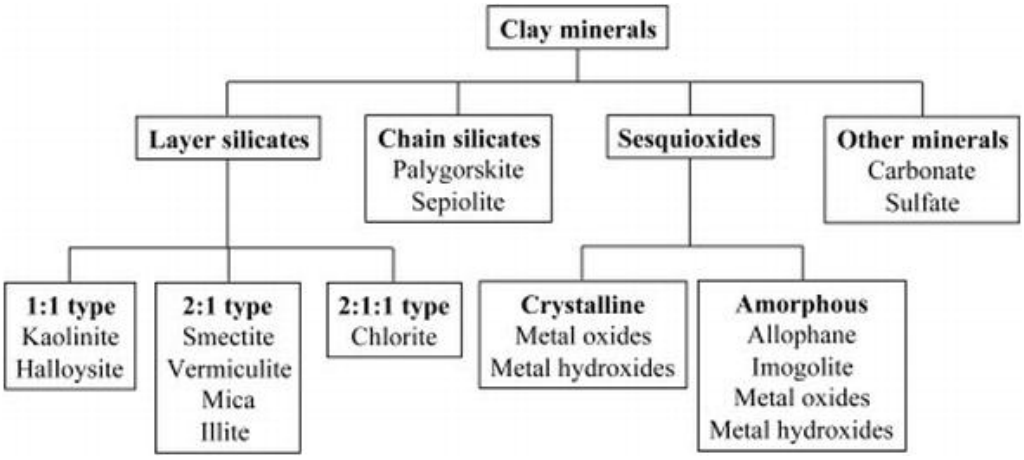

Figure 2.1. Illustration of the classification of different clay minerals. Edited from [10].

2.1.1.1 Layer silicates

These silicates are planar layers of tetrahedrals and octahedrals with repeating distances between the layers. Based on the number of layers, they can further be classified into 1:1-, 2:1- and 2:1:1-structures[11]. The structures can be observed on Figure 2.2.

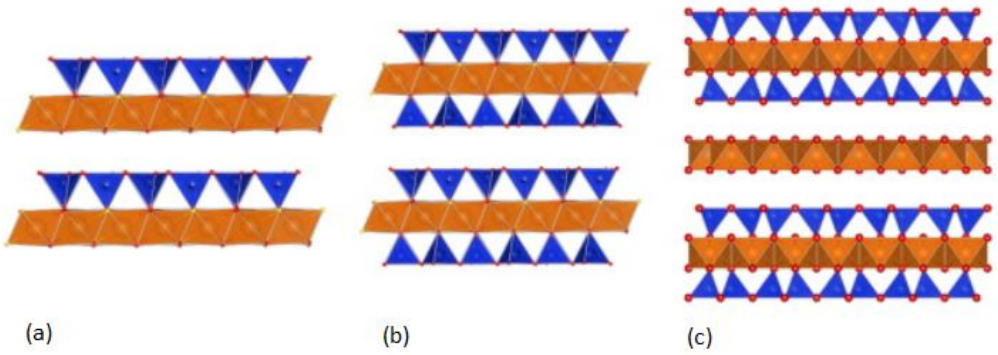

Figure 2.2. Visualization of: (a) 1:1 structure of phyllosilicates, (b) 2:1 structure of phyllosilicates (c) 2:1:1 structure of phyllosilicate. Edited from [12].

1:1 layer silicates is a simple conformation of one tetrahedral and one octahedral sheet bonded via sharing apical oxygen atoms[10].

2:1 layer silicates are structured with one octahedral sheet sandwiched between two tetrahedral sheets, forming what is known as the 2:1 layer. These layers are connected by interlayer ions and sometimes water, depending on whether the clay minerals are classified as expanding or non-expanding.
In the case of expanding clay, the attraction between the layers is influenced by oxygen atoms in the tetrahedral layers, along with the presence of water and cations in the interlayer space. This water content is key to the clay's ability to swell and shrink, as well as its capacity for cation exchange. Non-expanding clay, on the other hand, has a high negative charge in its tetrahedral layer, which is offset by positively charged ions that are located between the layers. This arrangement maintains the integrity of the layers

and inhibits expansion. These differences in how the layers are bonded result in various effects, such as a reduction in the size of the interlayer space and a decrease in the ability of adsorption, swelling, shrinkage, and cation exchange compared to expanding clay, although still greater than what is seen in 1:1 structured clays [10; 11].

2:1:1 layer silicates clay is composed of 2:1 layers with a magnesium dominated trioctahedral sheet between each 2:1 layer, creating the 2:1:1 structure. The structure is held together by the negative charge in the tetrahedral sheets and the positive charge in the trioctahedral magnesium sheets. The 2:1:1 structure has no water adsorption between the layer and is thereby non-expanding[10; 11].

2.1.2 Structure of clay

Clay minerals are mainly composed of oxides from a variety of ions. These oxides are arranged into two types of basic crystalline units: The tetrahedral sheet and the octahedral sheet.

2.1.2.1 Tetrahedral and octahedral sheet structure

The basic building block of the tetrahedral sheet is a Si-atom surrounded by four oxygen atoms, known as a silica tetrahedral unit cell, as seen in Figure 2.3 (a). The tetrahedral sheet is formed by sharing three oxygen atoms of each tetrahedral with the three nearest tetrahedrals, as it is shown in Figure 2.3 (b).

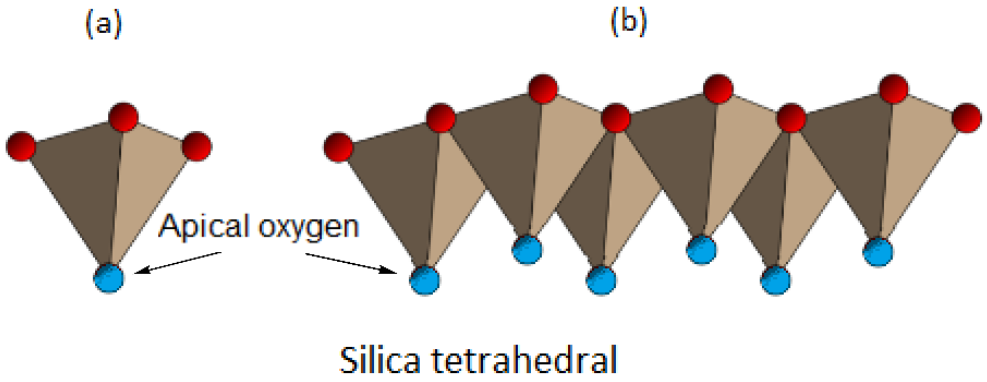

Figure 2.3. (a) Structure of a silica tetrahedral unit cell and (b) Arrangement of tetrahedral units to form the tetrahedral sheet. Edited from [13]

The connecting oxygen atoms are known as basal oxygen, which connects pairs of silica tetrahedrals in one plane, whereas the fourth oxygen of each tetrahedral remains free. The fourth oxygen atom is known as an apical oxygen atom, as it is in a separate plane providing a link between the tetrahedral- and octahedral sheets. As there is only one apical oxygen atom present per tetrahedral, as seen in Figure 2.3, each tetrahedral therefore shares a corner with an octahedral in the octahedral sheet[10; 14].

The octahedral sheet predominantly consists of Al^{3+} or Mg^{2+} ions surrounded by six O-atoms or OH-groups. Depending on the most abundant atom, the structure of the sheet changes. The structure can be different forms of octahedral sheets. A dioctahedral sheet occurs if Al^{3+} is the most common ion. This 3+ valence of the ions corresponds to only two-thirds of the unit cell being full, so the charge is balanced making the unit cell $Al_2(OH)_6$, where the two Al^{3+} are in coordination with a total of six oxygen or hydroxyl ions. Through this process, the structure forms a dioctahedral. When the sheet primarily consists of Mg^{2+}, three Mg-ions are necessary to balance the unit cell which has the formula $Mg_3(OH)_6$ thereby forming a trioctahedral structure. Every unit cell forms the di- or trioctahedral sheet by sharing two O-atoms with each adjacent unit cell, thereby connecting them into sheets[10; 14], which is shown in Figure 2.4 (b) and (c).

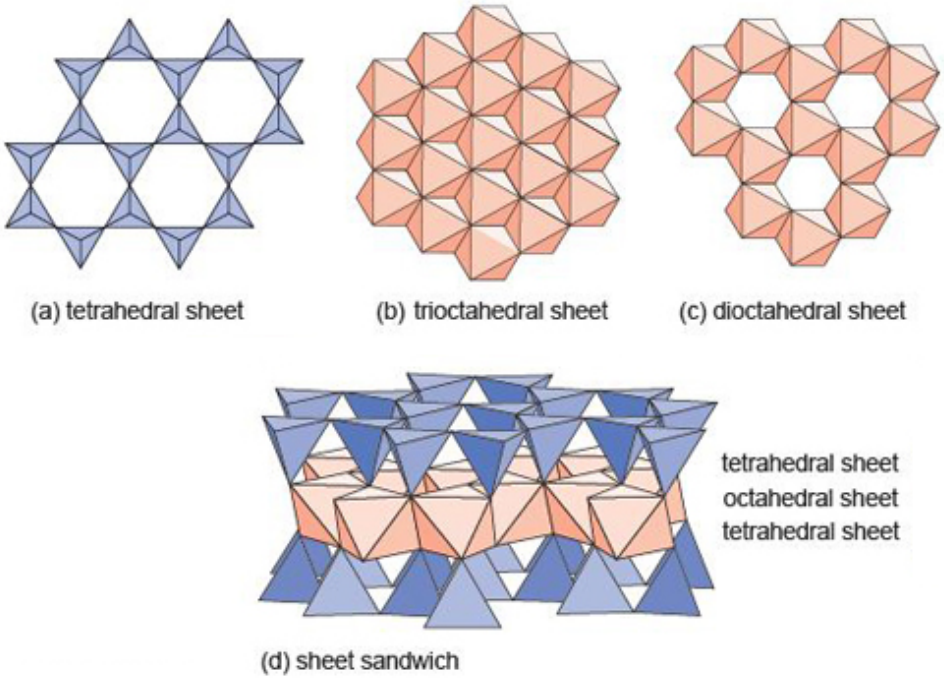

Figure 2.4. (a) Structure of tetrahedral sheet, (b) structure of trioctahedral sheet, (c) structure of dioctahedral sheet and (d) the clay forming sheet sandwich structure. Edited form [15]

.

Figure 2.4 (d) shows the sheet sandwich which forms clay, consisting of tetrahedral and octahedral sheets connected by an apical oxygen from the tetrahedral sheet.

The overall charge in tetrahedral or octahedral sheet clay is mainly a product of isomorphic substitution. The previously described unit cells, $Al_2(OH)_6$ and $Mg_3(OH)_6$, can be altered through the substitution of Si^{4+}, Al^{3+}, and Mg^{2+} with other cations of similar size. The substitution ions can have a different charge than substituted ions, hence a charge deficiency or excess is generated. The overall charge of the clay can be determined by balancing the electrons added or subtracted from the structure[16].

2.1.2.2 Other clay structures

Chain silicates differ from the former sheet silicates, in the sense that no network is formed and therefore, the silicates do not form a sheet, but instead a chain where the tetrahedral only shares two O-atoms instead of the three O-atoms shared in a sheet. Each chain is held together by ionic bonds to cations via balancing the charge of the chain silicates, and this structure is also illustrated in Figure 2.5. The open structure also provides a high cationic exchange of the Si-atoms with other cations such as Fe-, Mg-, and/or Ca-ions[17; 18].

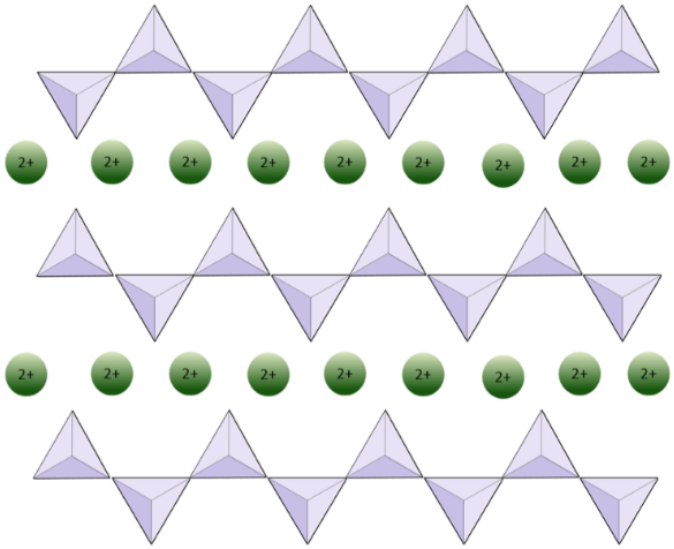

Figure 2.5. Illustration of the structure of chain silicate tetrahedrals bound together by cations[17].

Sesquioxid clay is naturally produced when rain leaches most silica and alumina out of the clay. This leaves behind the less soluble Fe_2O_3, $Fe(OH)_3$ and $Al(OH)_3$ compounds. Sesquioxid generally consists of three O-atoms and two other elements, typically metal atoms with valence 3+. They are also often characterized by not swelling in water, typically having large amounts of phosphate and low cation exchange capacity. Sesquioxid can be found as crystalline structures composed of metal- or hydroxide, or as amorphous structures comprised of allophane and imogolite[10; 19].

2.1.3 Kaolinite

Kaolinite ($Al_2Si_2O_5(OH)_4$), is the primary component of kaolin clay, possessing a well-defined 1:1 layer structure. This structure consists of alternating sheets: a tetrahedral sheet of silica $[Si_2O_5]^{2-}$ and an octahedral sheet of alumina $[Al_2(OH)_4]^2$. Raw kaolinite found in nature has impurities in the form of quartz, mica and in less frequently contains compounds as illite, feldspar, montmorillonite and many more. When heated to $\approx$ 420 °C, the kaolinite undergoes dehydroxylation, releasing its $2\,H_2O$ resulting in a minor shrinkage and weight loss. This new phase is know as metakoalinite ($Al_2Si_2O_5$). On further XRD analysis, metakaolin shows a more amorphous structure, which indicates

a structural disturbance through the dehydroxylation. Illustrated below, a more precise arrangement of the atoms can be seen in Figure 2.6 [6]

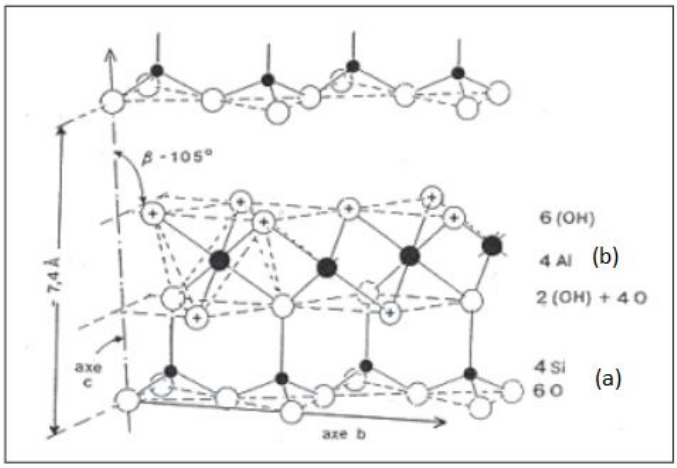

Figure 2.6. Illustration of the crystal structure of kaolinite, showing both tetrahedral (a) and octehedral (b) formation. Edited from [6].

2.2 Glass

The glass utilized in this project, is made of oxides. Most oxide glasses are optically transparent, but can also be semi-transparent through the presence of chalcogenides and transition metals, that can color the glass slightly. Glass can have different compositions, depending on what it has to be used for. Still, the main components to make glass are mainly the same. Even though glass is known to be a brittle material, it not only can be quite strong under the right conditions, but is also in this project used mainly for its components and structure

2.2.1 Composition and formation

Diving deeper into the composition of oxide glasses, the four primary oxides used are silicates (SiO_2), borates (B_2O_3), phosphates (P_2O_5), and germanates (GeO_2). In these groups, the ions Si^{4+}, B^{3+}, P^{5+} and Ge^{4+} are considered network formers, and the rest of the elements, are mainly split into the three groups; network modifiers, intermediates, and colorants[20]. Examples of different ions, oxides, and their functions are shown in Table 2.1.

Table 2.1. The different ions and oxides of glass[20].

Group	Ions	Oxide form
Network modifiers	Li^+, Na^+, K^+, Ba^{2+}, Mg^{2+}, Ca^{2+}	Li_2O, Na_2O, K_2O, BaO, MgO, CaO
Intermediates	Al^{3+}, Pb^{2+}, Ti^{4+}, Zn^{2+}	Al_2O_3, PbO, TiO_2, ZnO
Colorants	Cd^{2+}(red), Co^{2+}(blue), Cr^{3+}(green), $Cu^{1/2+}$(cyan), $Fe^{2/3+}$(brown), $Mn^{2/4+}$(magenta)	CdO, CoO, Cr_2O_3, CuO, Cu_2O, FeO, Fe_2O_3, MnO, MnO_2

Network modifiers are alkali or alkaline earth ions, that reside in the interior void spaces, but are not a part of the primary network. The second group **intermediates** are capable of penetrating an already existing network, but can not by themselves create a network. The third and last group are **colorants** and these impurity ions have the ability to absorb light at a specific wavelength, to color the glass[20].

When producing glass, raw material needs to be heated, until it changes into a liquid phase. To turn a material into a glass it has to be heated over its melting temperature (T_m) so it becomes a liquid. Then the liquid needs to be cooled rapidly so that it reaches its glass transition temperature (T_g). T_g is defined as the low temperature where the liquid gets solidified to an amorphous solid after being cooled down rapidly and is thereby dependent on the cooling rate[20]. Because of the rapid cooling, the liquid becomes a supercooled viscous liquid at a temperature below its T_m. Thereby, the atoms do not have enough time to structure themselves properly in a crystalline state and hence become amorphous. If the heated material is not cooled rapidly enough to reach T_g, there are instead formed crystals at the T_m. If materials that are mixed differ in their T_m, the T_m of

the mix becomes a product of the mixture and hence differs from different compositions. One of the biggest challenges of producing glass is the melting of the material, which can occur at very high temperatures. The T_m can be lowered by the addition of fluxing agents or network modifiers. A fluxing agent typically works by lowering the eutectic temperature and the viscosity of the melt[20]. A common fluxing agent in glass is calcium carbonate, $CaCO_3$, which turns into CO_2 and CaO at a lower temperature than the T_m of the glass materials[21]. CaO is by itself a network modifier that disrupts the highly connected network, commonly of ${SiO_4}^{4-}$, by introducing non-bridging oxygen[20]. The network modifier, which is an ionic oxide, dissociates inside the glass where the strongly electropositive cation has an affinity for the electronegative oxygen atoms. One of the covalent bonds, connecting the bridging oxygen atom to the rest of the network, is therefore broken by the cation. The cation then binds itself to the newly non-bridging oxygen and the network is broken. The breaking of the network shortens the continuous network chain, and as the chains get shorter they can slide past each other more easily during cooling. Therefore, the volume inside the glass is lowered, because the shorter chains can pack more efficiently thereby lowering the T_m[22].

When comparing the structures of crystals and glass, the crystals have a long-range order, where the fixed structure is repeated throughout the compound due to the arrangement of atoms. This means that there is a fixed number of coordination atoms, uniform bond angles, and bond lengths. Glass on the other hand, has its atoms arranged in a random network. Even though the nearest neighbor bond distance, coordination number, and some bond angles are mainly fixed, the network is considerably composed of a short-range order, where the structure throughout the compound changes, and thereby does not have one set structure with repeating units[20].

2.2.2 CAS-glass

CAS glasses, generally represented by the formula $CaO{-}Al_2O_3{-}SiO_2$, are modified silicate glasses. Their structure and properties are strongly influenced by the relative proportions of their constituent oxides, especially the CaO/Al_2O_3 ratio (R). This ratio is a critical determinant of network structure and overall material properties. Near-metaluminous compositions ($R \approx 1$), analogous to mineral anorthite ($CaAl_2Si_2O_8$), typically exhibit a relatively well-ordered network structure.

Aluminum is predominantly four-fold coordinated (Al^{4+}) within the silica network (SiO_4 tetrahedra). This near-stoichiometric balance results in a highly polymerized network with few non-bridging oxygens. Strong electrostatic interactions between Ca^{2+} and Al^{3+} ions effectively compensate for the charge imbalance created by aluminum substitution. This structural arrangement is often considered representative of normal CAS glass. slight variations in oxide percentages can still yield largely ordered structures.

In contrast, peralkaline CAS glasses (R significantly $\gg 1$) display different characteristics. The disruption of charge balance leads to a less-ordered structure with a higher concentration of non-bridging oxygens and potentially tri-clustered oxygens. The

aluminum avoidance principle (minimizing Al−O−Al linkages) is frequently violated [4], resulting in more Al−O−Al linkages. These structural changes directly influence network connectivity, bond strengths, and overall material properties. [23; 24; 25; 26]

2.3 Portland Cement

Portland cement's exceptional performance as a construction material derives from its chemical composition and complex microstructural change during hydration. This section dives into the fundamental chemistry behind its manufacturing, the key compositional phases, and their interactions during the hydration process.

2.3.1 Clinker Formation

Portland cement production begins with a carefully controlled blend of raw materials. These raw materials typically include calcium-rich sources like limestone, which provides the necessary calcium oxide (CaO) 67%, and aluminosilicate clays, offering silicon dioxide (SiO_2) 22%, aluminum oxide (Al_2O_3) 5%, and iron oxide (Fe_2O_3) 3% where the last 3% consist of other components. The exact ratios of these components are critical, which dictates the final properties of the cement. [27]

To achieve this blend of oxides, all the raw materials gathered, except the soft materials, have to firstly be crushed and ground. This is typically done in rotating, cylindrical ball, or tube mills, containing steel balls, which grind the raw materials inside. [28]

This carefully balanced mixture undergoes high-temperature processing in a rotary kiln, where the raw materials are fed from the top of the kiln, with rotation and a slight incline, to ensure that the raw materials can pass through to the bottom, also known as the firing end. The process consists of two key stages: **calcination**, the thermal decomposition of limestone $CaCO_3 \longrightarrow CaO + CO_2$, followed by clinkering. **Clinkering** involves partial melting at temperatures around 1450 °C, leading to the formation of four primary crystalline phases. The phases in question are alite (Ca_3SiO_5), belite (Ca_2SiO_4), aluminate (Ca_3AlO_6), and ferrite (Ca_2AlFeO_5) denoted respectively as C3S, C2S, C3A and C4AF. [27; 28]

It is crucial to note that clinker formation is a highly dynamic non-equilibrium process. The final phase assemblage and the chemical composition of each phase are significantly influenced by reaction kinetics, including the raw materials' time under high temperatures, homogeneity, and the specific operational parameters of the rotary kiln. After clinkering, the resulting clinker undergoes fine grinding, adding $\approx$ 5% gypsum ($CaSO_4 \cdot 2\,H_2O$) to regulate the setting time and initial strength gain of the cement. An overview of the different phases, under different temperatures can be observed on Figure 2.7, showing the theoretical amount of the 4 main phases, and the components which have not reacted. It has to be noted, that this is not a true representation, but a theoretical illustration. [29]

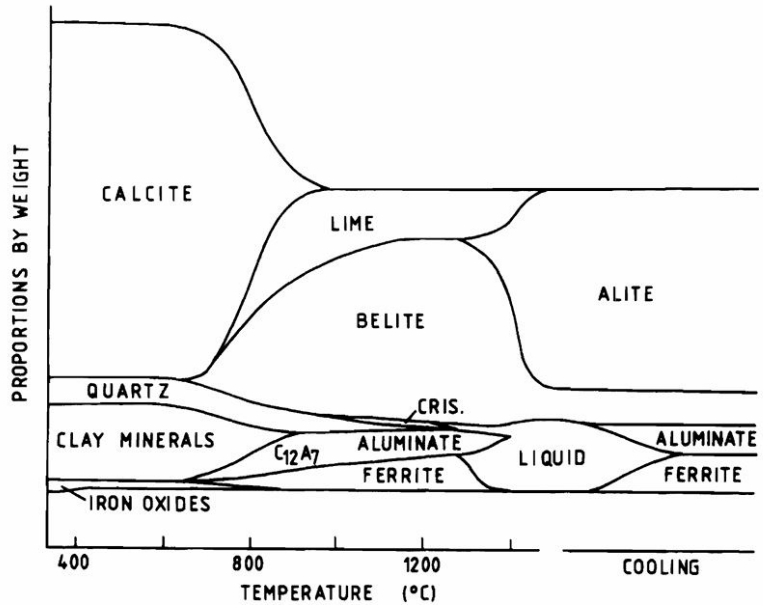

Figure 2.7. Illustration of the different phases in weight, based on temperature. Edited from [29].

Alite, typically the most abundant phase in clinker (50-70%), is the primary driver of early-stage strength. Its hydration process runs relatively quickly, where 70% of C3S is reacted after 28 days, resulting in calcium hydroxide (CH) and calcium silicate hydrate (C-S-H) as products, the primary binding agent in hardened cement paste. The chemical composition of alite, however, is not fixed. In pure clinker C3S has 73.7% CaO, and 26.3% SiO, but there is usually found 3-4% substituents, where the most relevant substituents are in form of $Mg_2{}^+$, $Al_3{}^+$ and $Fe_3{}^+$ ions. Here there is evidence on MgO replacing CaO, which significantly influences its hydration rate and the properties of the resulting C-S-H gel. Moreover, the existence of different alite polymorphs further complicates the reaction kinetics.

Belite which is 15-30% of clinker hydrates much more slowly than alite, contributing significantly to long-term strength and durability, and less to the early strenght. Pure C2S consist of 34.9 % of SiO_2 and 65.1 % CaO. C2S typically contains 4-6 % substituent oxides in form of Al_2O_3 and Fe_2O. Its slower reactivity stems from its more stable crystal structure. Nevertheless, belite hydration also produces $C-S-H$ gel, but much less CH.

Aluminate plays a critical role in setting time, even though it is only presented in smaller amounts (5-10%). Its rapid reaction with water can cause undesirable flash setting if not carefully controlled. The addition of gypsum is here essential, reacting with aluminate to form ettringite, a sulfate-containing hydration product that significantly retards the hydration process and prevents premature setting.

Ferrite, the least abundant of the four major phases (5-15%), is a slower-hydrating phase with a more complex influence on cement properties. It has a relatively minor contribution to strength development but significantly impacts the color of the cement. The Al^{3+}/Fe^{3+}

ratio within the ferrite phase and the presence of other substitutional ions further modulate its hydration behavior. The strength gain observed in Portland cement comes from the complex hydration reactions of its constituent phases with water. The kinetics of this process are governed by several joined factors, most significantly the properties of the individual phases and their interactions.[27; 29]

2.3.1.1 Bogue calculation

The amount of the four major phases in cement clinker, can be calculated from the Bogue calculation. The equation assumes that there is only pure C3S, C2S, C3A and C4AF present in the final clinker. The clinker is formed, by the reaction between $CaCO_3$ and SiO_2, and $CaCO_3$ with Al_2O_3. For the purpose of the calculations, the unreacted $CaCO_3$ has to be subtracted from the total amount before the calculations are performed. The Bogue calculations can be done, with four simple steps, but it is important to note, that in the industry, the raw materials used differ slightly in composition, and are not as assumed pure. C4AF is the only phase that contains iron, which fixes the amount of C4AF making it a good starting point. Then C3A can be calculated by subtracting the amount of Al_2O_3 in C4AF, with the total amount in the clinker. Subsequently, it is assumed that all SiO_2 in the clinker is present as C2S, which can be used to calculate how much CaO is needed to form C2S from the total amount of SiO_2. This will lead to a surplus of CaO. Lastly the surplus of CaO is allocated to C2S, converting parts of it to C3S. This gives a good estimate on the wt% of the different oxides in clinker:

$$C_3S = 4.0710 \cdot C - 7.6024 \cdot S - 1.4297 \cdot F - 6.7187 \cdot A$$

$$C_2S = 8.6024 \cdot S + 1.0785 \cdot F + 5.0683 \cdot A$$

$$C_3A = 2.6504 \cdot A - 1.6920 \cdot F$$

$$C_4AF = 3.0432 \cdot F$$

It is important to note, that there are ways to adjust Bogues calculations, since it by itself it not applicable. It is for example not desired to have any unreacted CaO, in the case of cement, the lime saturation factor can be corrected by subtracting $0.7 * SO_3$ from CaO.

[30; 29]

2.3.2 Supplementary Cementitious Material

SCMs cover a wide variety of materials that can be used to partially replace Portland cement, to improve its properties while lowering the emission of CO_2. Some of the most implemented and researched materials are FA and GBFS, whereas materials such as dolomite also has been researched for the same use.

2.3.2.1 Fly ash and slag

By-products such as FA and GBFS have been a cornerstone in SCM research. FA is a waste material, obtained after burning solid fuels. It contains mainly unburned carbon and metal oxides in the form of SiO_2, Al_2O_3, Fe_2O_3, and SO_3. FA is useful since when it comes in contact with water, low-calcium FA reacts with C-H, resulting in C-H-S and calcium aluminates. The most important component of FA is the unstable silica-aluminum-potassium glass, a product of the combustion process. Here, the active SiO_2, is provided for the reaction with C-H under normal conditions to form C-H-S.

GBFS is a byproduct of crude iron production, in a blast furnace, reaching temperatures of 1500 °C. The process of melting waste rock of iron ore, flux (limestone, dolomite, etc.) and inorganic parts from the combustion of fuel, being carbonaceous components. Slag has a lower density than the other materials in the furnace, resulting it to flow over the surface of molten iron, if then quickly cooled down from 1400-1450 °C by a water jet, granulation occurs, making it ready to be used in cement or concrete. If water is not utilized, but the slag is left to cool with air, it crystallizes, rendering it much less useful as a component in cement. It shows, that the utilization of the components in GBFS in cement and concrete is above 90 %, where the utilization of fly ash is only around 30 %. [5; 31]

2.3.2.2 Dolomite

Dolomite ($CaMg(CO_3)_2$) is known as a double carbonate, theoretically consisting of 54.35% $CaCO_3$ and 45.65% $MgCO_3$ in its pure form. When calcined, depending on the purity of dolomite the decomposition temperatures can differ. Under thermal decomposition 2 major phases are observed, where Shahraki, B.K., et al. [32] had found the first phase (Equation 2.1) at 772°C, to be the release of CO_2 from $MgCO_3$, followed by the second phase (Equation 2.2) 834 °C, which is a decomposition of $CaCO_3$, resulting again in the release of CO_2

$$CaMg\,(CO_3)_2 \rightarrow CaCO_3 + MgO + CO_2 \tag{2.1}$$

$$CaCO_3 \rightarrow CaO + CO_2 \tag{2.2}$$

It is mainly utilized in the ceramic, glass, and steel industries, where the dolomite used in the steel industry is preferred to have small impurities in the form of silica and iron [33]. The crystal lattice structure in dolomite consists of altering layers of Ca and Mg, separated by layers of CO_3, which can be observed on Figure 2.8 [34]

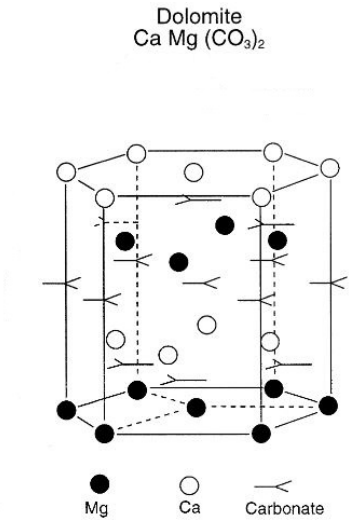

Figure 2.8. Illustration of the ideal crystal lattice structure in dolomite. Edited from [34].

When implemented in low amounts, dolomite can have a positive effect as an SCM. A study by Szybilski, et al., [35] shows that it for example can accelerate the hydration of C3S, when implemented in amounts of around 5-15%, whilst not retarding the setting of paste. According to Caceres, P.G [36] extensive grinding of dolomite can disturb its crystal lattice structure, thereby influencing the decomposition, and introducing the two Mg-species, known as Mg-I and Mg-II, where the decomposition temperature of these have a difference of ≈ 100 °C. [36]

Method contemplations 3

This chapter will explain the considerations behind the different analysis and methods used throughout this project. Some have been inspired solely by literature, whilst others have been adjusted for the sake of convenience.

3.1 Preparation of samples

The raw materials worked with in this project are all fine powders, to ensure homogeneity, the raw materials weighed for both the CAS- and calcium magnesium aluminosilicate (CMAS) glass, but also the clays, are put in a blue cap bottle and shaken by hand. After that, the sample is put through a sieve shaking machine with 2 compartments, 500 µm and 250 µm. This is done once to twice per composition, depending on how well the powders pass through the initial 500 µm sieve. This can vary from the amount of sample that is put through the sieve shaking machine. Depending on the material, approximately 5 min of sieving is needed for each composition used.

3.2 Synthesis of CAS and CMAS-Glasses

For the synthesis of glasses, a furnace is required to reach temperatures of 1500-1600 °C, ensuring that the materials are fully melted and form a homogeneous liquid. In this project, the focus is only on the structure and components used in both CAS and CMAS glass, making the shape and formation of bubbles less significant. Therefore, a straightforward quenching process is utilized in which all of the molten glass is dumped into a bucket of room-temperature deionized water, ensuring that no impurities occur during the quenching process. Quenching must be performed rapidly to prevent crystal formation while ensuring the formation of an amorphous structure. The stresses introduced by the quenching process enhances the surface hardness of the glass. To address this hardness, the glass has to be ground using a ball mill, with a ZrO_2 jar where 8-10 aluminum balls are added. The ZrO_2 jar is used, as materials such as steel would introduce impurities in the glass when ground. The glass has to be ground to a powder, to sieve the samples in the range of 125 - 64 µm, for later use.

It should be noted that Platinum-rhodium crucibles possess a high melting temperature, coupled with greater resistance to oxidation and corrosion, ensuring that they do not introduce impurities into the glass. This makes them well suited for the formation of CAS/CMAS-glss.

The materials used for making glass contain carbonates, which decompose under the various temperatures producing gasses. This can make the volume of the material exceed the volume of the crucible. Hence, the furnace is firstly sat on 900 °C, where after the raw material for the glass is poured into the crucible gradually, leaving space for gasses to escape, shrinking the the amount of sample in the crucible, leaving space for more material. This is done until all the material has safely decomposed. Hereafter the temperature is raised gradually from 900 °C to 1500 °C, ensuring that all the material have had enough time on each temperature step, to fully decompose and become homogeneous. When no change is observed to the material in the crucible at around 1200-1300 °C, the temperature can gradually be raised to 1500 °C and left for 2 h for the CAS-glass. CMAS-glass has a higher melting temperature, which requires 2 h on 1600 °C.

3.3 Thermal treatment of clays

For the thermal treatment of clays, a furnace has to be utilized that can reach temperatures of 900 °C. For the sake of convenience, water is gradually introduced to the fine powders, which makes the materials dough like, allowing the materials to be formed into small balls by hand. The amount of water is not defined, but is added until the materials can be molded by hand. This is done for convenience, so that the samples can be calcined, without the use of molds. By forming the dough into small uniform balls, the calcination conditions for the materials are held the same.

3.4 Mechanochemical activation of clays

For mechanochemical activation (MA), it is important that the procedure for all materials is as identical as possible. For this purpose, the same ball mill jar, together with its aluminum balls, and the amount of sample is held the same. The goal for loading the samples was wished to be 1/4 of the jar, ensuring that all the material gets equally grinded.

3.5 Analysis of materials

For the analysis methods utilized in this project, it is important to again ensure homogeniety. Since small changes can impact the results. For the samples that have been through mechanochemical activation, there might be a difference in structure between the powder which is free in the bottom of the ball mill container, and the material which is stuck to the sides after a run. Therefore, before utilizing the XRD for the mechanochemical activation, the sample has to be mixed, and stirred around, but not additionally ground.

3.5.1 XRD

The XRD is mainly utilized, to get a better understanding of the materials worked with. With the XRD, the different crystalline phases in the sample can be identified, and hence if any change occurs. With the help of the XRD, a correlation is wished to be found, between the degree of crystallinity compared to amount of bound water.

3.5.2 DSC

By a heating rate of 10 °C / min, to 580 °C a phase change is observed, showing the amount of bound water which is evaporated. Since gas is produced by the release of bound water, the lid of the crucible is pierced with a needle, so the gas produced can escape.

3.5.3 LS

With the LS 13 320 Laser Diffraction Particle Size analyzer, the size of the particles are wished to be known, after they have been ground in the ball mill. For the model, water is chosen with a refractive index of 1.33, with the refractive index of the materials to be 1.60, since 1.60 falls in the range of all the materials analyzed. The pump speed is set to 12%, and the program is set to rinse, de-bubble, align, and measure background, between each run. To ensure the apparatus is measuring correctly, each run is composed of 3 individual scans, giving the values of D50 and D90 as an average of the 3 scans. Each sample has to be put in an ultra-sound bath for 30 min, so that the particles do not stick together, resulting in an imprecise particle size analysis.

Experimental methods 4

This chapter will describe the methods used for the experimental procedures conducted in this project. The methods are undertaken to find the different effects CAS and CMAS-glass, Co-calcined clays and MA materials have as an SCM. Before any method or analysis is conducted, it is important to note, that all the samples are prepared with regard to the contemplation section. The sample ID and different compositions used in this project are measured in accordance to the mol% in Figure 4.1

Sample	Sample ID:	T(°C)	CaCO3	Dolomite	Al2O3	SiO2	Kaolinite
CAS-Glass	CAS_25	1500	25		25	50	
	CAS_40	1500	40		20	40	
	CAS_55	1500	55		15	30	
CMAS-Glass	CMAS_40	1600		40	20	40	
Metakaolin	MK_700	700					100
	MK_800	800					100
	MK_900	900					100
Ca-MK	Ca_MK_700	700	40				60
	Ca_MK_800	800	40				60
	Ca_MK_900	900	40				60
Ca-MK	Ca_MK	MA	40				60
Kaolin + Dolomite	Dol + Kao	MA		40			60

Figure 4.1. Table of mol% used in this project, with the different components and sample ID.

4.1 Synthesis of CAS and CMAS-Glasses

The components are measured using the Ohaus Scout precision scale, mixed, and poured into a 50 mL platin-rhodium crucible, so that only 2/3 of the crucible is filled. The weighed components can be seen in Table 4.1

Table 4.1. The materials and amount necessary to get $30g$ of raw materials for synthesizing CAS and CMAS Glass

CAS & CMAS Glass				
Components	$CaCO_3$	Dolomite	Al_2O_3	SiO
CAS_25	9.3188		9.4932	11.1878
CAS_40	14.2204		7.2432	8.5362
CAS_55	18.6886		5.1922	6.1191
CMAS_40		18.7233	5.1763	6.1003

The crucible is placed in the furnace and the heat is turned to 900 °C. The remainder of the sample is gradually added to the crucible, in accordance to the material being calcined.

When all the measured sample has been placed in the crucible, the heat is turned to 1200 °C for 30 min. For the CAS-glass the temperature is afterwards gradually raised to 1500 °C for 2 h, whereas the CMAS-glass is raised to 1600 °C for 2 h. The molten glass is then quenched in a large bucket filled with room temperature demineralized water prepared beforehand. The glass is then collected and dried at 105 °C.

4.2 Thermal treatment of clays

The materials are measured with the Ohaus Scout precision scale, and transferred to a 600 mL beaker. In the same beaker, demineralized water is added, until the powder becomes dough like. The dough like substance is formed by hand to similar sized balls, placed in aluminum containers, and then put in a drying oven until dried. The now dry balls are transferred to $50ml$ high aluminum crucibles, and calcined for 2 h at temperatures of respectively 700, 800 and 900 °C. The compositions and temperature used can be seen in Table 4.2

Table 4.2. The materials and amount necessary to get $30g$ of sample after calcination of kaolin and Ca-kaolin

Components	T(°C)	Kaolin	$CaCO_3$
Kaolin	700	35.49082	
	800	35.49082	
	900	35.49082	
Ca-MK	700	30.38176	7.71338
	800	30.38176	7.71338
	900	30.38176	7.71338

4.3 Mechanochemical activation of clays

The materials used are measured with the Ohaus Scout precision scale, mixed if necessary, and transferred to small sealed containers. The materials are placed in the Planetary ball mill PM 100 using a 50 ml ZrO_2 jar where 8-10 aluminum balls are added. For each composition, 6 runs are performed, where the speed of the ball mill is 600 RPM, incrementing the run time with 20 min for each sample. An example of kaolinite can be seen in Figure 4.3

Table 4.3. Mechanochemical activation of kaolinite through a planetary ball mill

Kaolinite [3g]	Time [min]	Speed [RPM]
1.	20	600
2.	40	600
3.	60	600
4.	80	600
5.	100	600
6.	120	600

The same procedure applies to the other materials. The other materials in question are $CaCO_3$, Dolomite, Ca-Kaolin, and Dolomite + kaolinite, The tabulars for these can be seen in Appendix A. With the only difference, of $CaCO_3$ samples being weighed to 5g for all 6 runs. After each run, the ball mill jar is cleaned with water and ethanol. If water and ethanol are insufficient, a ball mill program with sand is used at 150 RPM for 15 min.

4.4 Reactivity test

Firstly, all the SCMs are sieved to a size between 124-64 µm with a sieve shaking machine at an amplitude of 1.5 mm for 3 min. The same ratio between the SCM, Calcium hydroxide, water, Potassium hydroxide, and potassium sulfate is kept for all samples. The ratio in question can be observed in Table 4.4

Table 4.4. Component ratio for reactivity test

SCM [g]	$Ca(OH)_2$ [g]	K_2SO_4 [g]	KOH [g]	water [ml]
1	3	0.13	0.012	4.8

For 10 samples at a time, 48 mL of water is poured in a 250 mL blue cap bottle, together with 1.3g K_2SO_4 and 0.12g of KOH, and stirred around until fully dissolved. Then for each sample, 1 g of SCM is firstly mixed with 3 g of calcium hydroxide in a plastic container, then 4.8 mL of the water solution is added to the powder and the mixture is stirred with a glass rod until homogeneous. The plastic container is sealed with a lid and parafilm. After 1, 7, and 28 days, 1/3 of the mixture is transferred to a beaker together with a magnet, and put on a magnetic stirrer. In the beaker, 25-30 mL of isopropanol is added and the beaker is sealed with parafilm. After an hour has passed, the magnet is removed, and the solution is put through vacuum filtration, until all the liquids are removed. All the dry sample is then collected in plastic containers, and put in a desiccator for 2 days. After the 2 days have passed, the containers are sealed tightly until further use. The measured amount of SCM and CH for all the materials can be seen in Appendix B.

4.5 DSC

An aluminum crucible is firstly weighed on the Ohaus precision scale together with its lid, then the powder is pressed into the crucible, ensuring that the bottom is covered and tightly pressed. The weight is again measured to obtain the weight of the sample. After the lid is secured on the crucible with a sealing press, a hole is poked on the lid with the tip of a syringe, before placing the samples on the autosampler. The weighed amounts of sample, pressed into the Al crucible can be observed on Appendix C

4.6 XRD

The powder is pressed into a sample holder and analyzed on the XRD-apparatus. The interval for the angle during the XRD analysis is set between 10,0025° and 80°, with a step

size of 0,01313°. The x-rays are generated with a copper source by the x-ray tube Empyrean Cu LFF HR (94300337310x). The tension and current are 45kV and 40mA respectively. The slits and mask used are an anti-scatter slit, fixed anti-scatter slit, divergence slit, and an incident beam mask with sizes of 7,5mm, 1/4", 1/4" and 10mm, respectively. To analyze the XRD diffractograms, the HighScore software is utilized to find the constituents corresponding to the peaks and analyze possible differences in the diffractograms.

4.7 LS

For each sample, pour $\approx 1/3$ of a spoon of material in a blue cap bottle, together with 20-30 mL demineralized water. Stir the blue cap bottle by hand before placing it in a ultra-sound bath for 30 min. After the ultra-sound bath, stir the bottle again by hand, before dripping the sample in the designated area, until the obscuration reaches 8-12%.

Results and discussion 5

In this chapter, the data obtained from the XRD, DSC, and LS analysis are examined and discussed. With the XRD, showing the structure and change in crystallinity between the samples, which can assist to get a better understanding of the data gathered from the DSC and LS.

5.0.1 XRD analysis

Through the Highscore software, different elements were identified for kaolin, to explain the peaks in the diffractogram, both before and after calcination, but also for the MA. Starting with a diffractogram of raw kaolin, it can be observed, that the sample contains small amounts of impurities in the form of quartz and illite, with kaolinte being the most abundandt component, which can be observed on Figure 5.1.

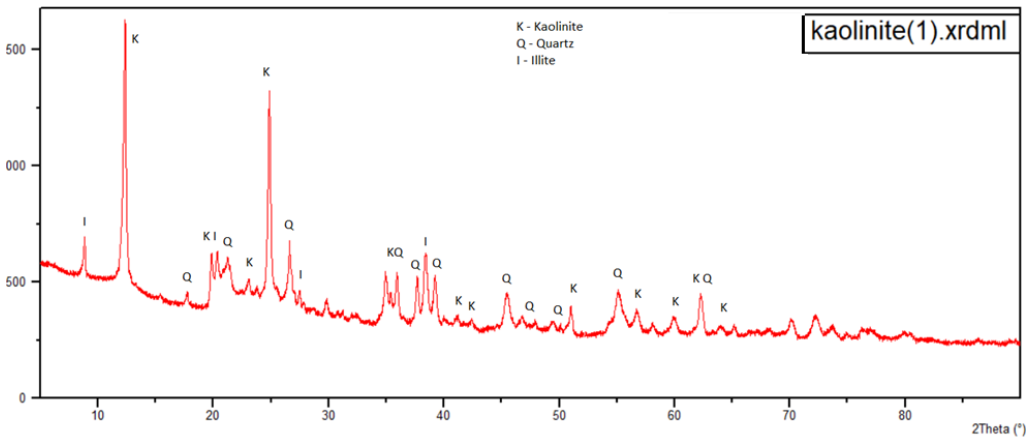

Figure 5.1. XRD - analysis of raw kaolinite

The exact purity of kaolin is wished to be determined, since the amount of impurities can have a significant impact on the reactivity. As mentioned in section 2.1.3, kaolinite undergoes dehydroxylation, releasing $2\,H_2O$ molecules under calcination resulting in the formation of metakaolin. Comparing the theoretical weight loss of pure kaolinite, with the measured weight loss, the impurity is calculated to 1.7718%, which makes the kaolin very pure, together with a calculations for Dolomite, which showed a purity of 100%. The calculations can be found in Appendix D

On Figure 5.2 the diffractogram of raw kaolin is compared with kaolin calcined at 700,

800, and 900 °C. The diffractogram of Kaolin expresses high crystallinity, but following calcination at the three different temperatures, it develops a significantly more amorphous structure consistent with the formation of metakaolin.

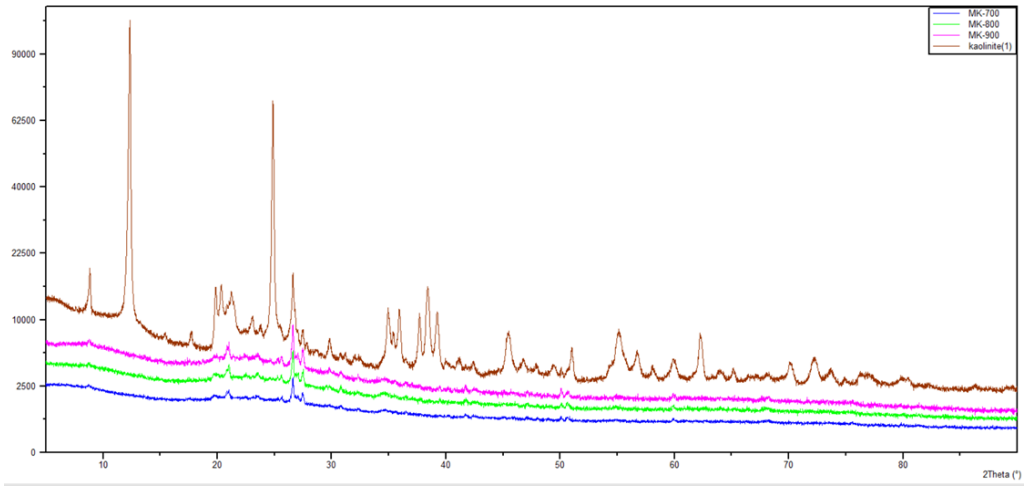

Figure 5.2. Comparison of raw kaolinite with calcined kaolinite at 700, 800, and 900 °C

Ca-MK was fired at the same temperatures as kaolin, showing the same pattern in Figure 5.3, which was observed for the calcined kaolin, becoming more amorphous.

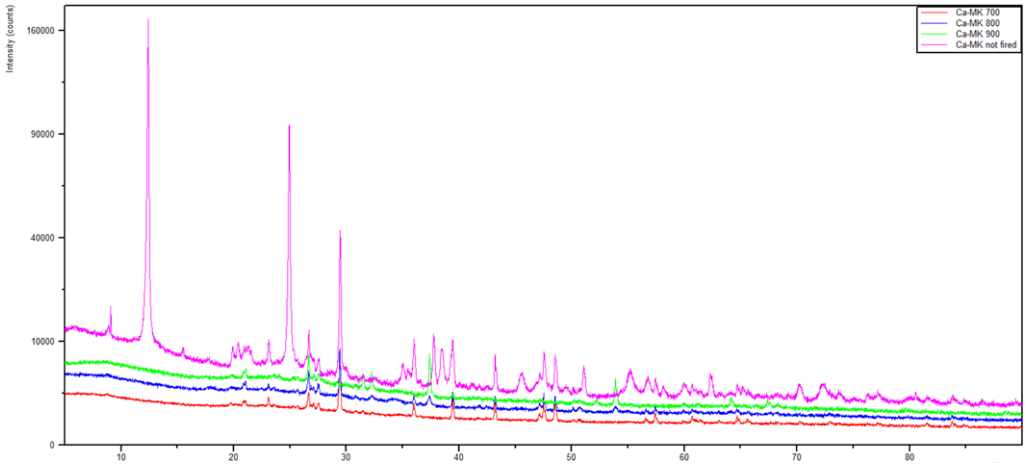

Figure 5.3. Comparison of raw Ca-MK with calcined Ca-MK at 700, 800, and 900 °C

The addition of $CaCO_3$ can also be seen, with the Ca-MK sample calcined at 700 °C, the decomposition starts taking place releasing CO_2 resulting in the formation of CaO. In line with the increase in temperature, firstly at 800 °C the sample becomes more amorphous as more of the $CaCO_3$ is decomposed, and together with the formation of CaO, new peaks are introduced. At 900 °C even more CaO is formed, showing an increase of intensities at the new peaks, making the sample more crystalline than the sample calcined at 800 °C.

For the MA samples, which have undergone grinding in a planetary ball mill for 20-120 min, it is not expected to yield the same results as for the calcined samples. However, since

the samples undergo extensive grinding, the long-range crystalline structure is disturbed, resulting in a more amorphous arrangement with the increase of grinding time.

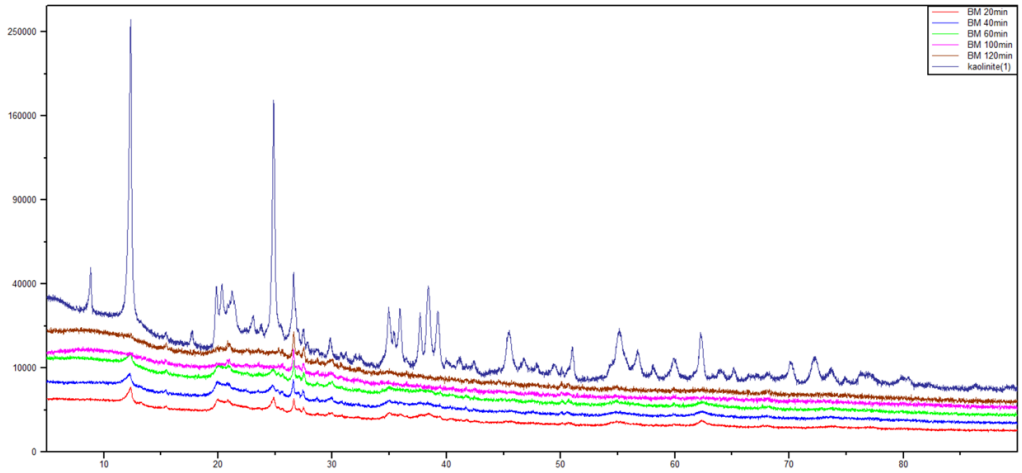

Figure 5.4. Comparison of raw kaolin with ball mill samples, ranging from 20-120min

Comparing the diffractogram on Figure 5.4 for the MA kaolin, to Figure 5.2 for the calcined kaolin, a very similar pattern is observed, with the kaolin peaks almost disappearing, and peaks that show similarity to the peaks of metakaolin start forming. Yet, similar diffractograms can not directly be linked to the samples being identical, since calcination has to occur, for the release of water and formation of metakaolin.

The diffractogram of both $CaCO_3$ on Figure 5.5 and dolomite on Figure 5.6 shows almost no difference in structure, when ground in a ball mill for 20-120 min, compared to the the samples where kaolin is added to both samples before grinding.

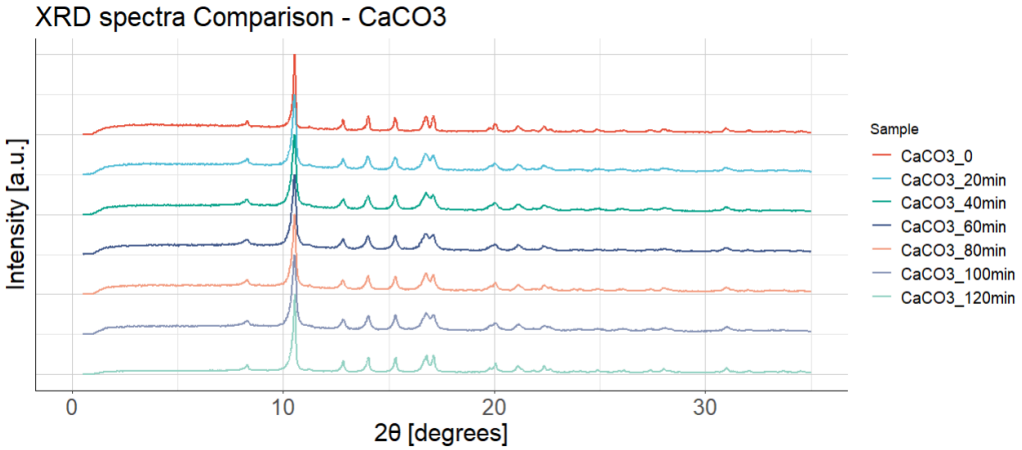

Figure 5.5. Comparison of raw CaCO3 with ball mill samples, ranging from 20-120min

When comparing the diffractograms of $CaCO_3$ with that of dolomite, similar peaks are observed, being a result of dolomite, as mentioned in 2.3.2.2, theoretically consisting of 54.35% $CaCO_3$ and 45.65% $MgCO_3$. The minor differences in peaks between $CaCO_3$ and $MgCO_3$, are not significant enough for there to be impurities and correspond with

the expected values. The diffractograms of pure $CaCO_3$ and dolomite can be observed in Appendix E, corresponding with the ball mill samples. Resulting in no significant change in structure.

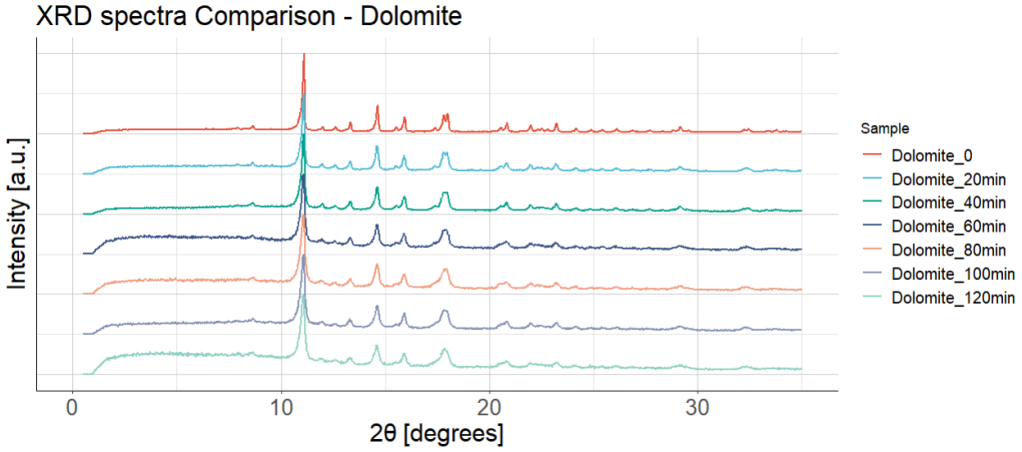

Figure 5.6. Comparison of raw Dolomite with ball mill samples, ranging from 20-120min

Comparing the structure of MA Ca-MK on Figure 5.7, with that of calcined Ca-MK on Figure 5.3, it can be concluded that the crystallinity does not show as much of a decrease when MA is performed compared to calcination. Which can be explained by the MA of $CaCO_3$ not changing in crystallinity, but rather the change is observed from the added kaolin.

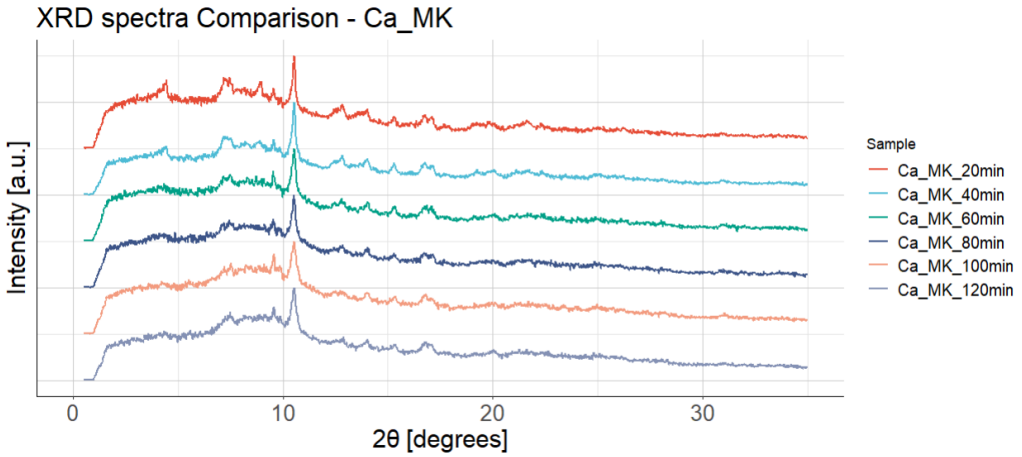

Figure 5.7. Comparison of Ca_MK ball mill samples, ranging from 20-120min

The Dol+kao samples on Figure 5.8 show a great change in crystallinity from the MA at all mill times, but with almost no change in structure with the increase of mill time, after 20 min of grinding. This partially correlates to the MA samples of kaolin in Figure 5.1. With the difference of 20, 40, and 60 min samples show similar patterns, whereas the kaolin samples get more amorphous at the mill times of 100 min and 120 min. The fact that less change is observed in these samples, could be correlated to the dolomite samples, which showed almost no change.

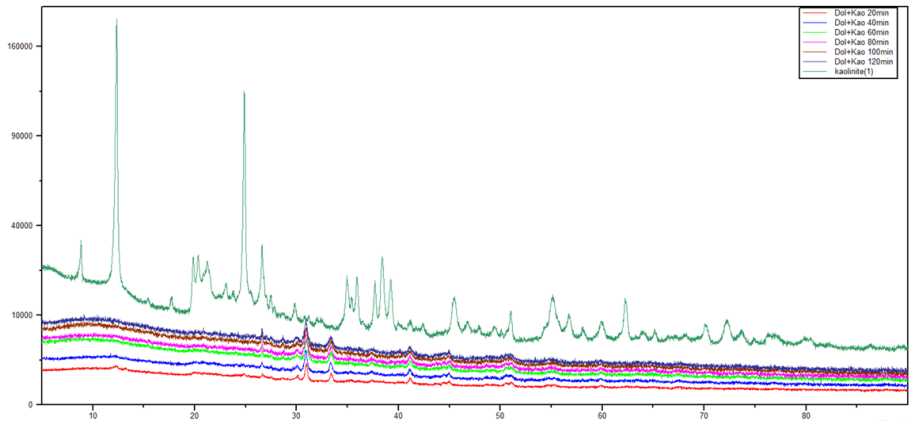

Figure 5.8. Comparison of Dolomite + Kaolin ball mill samples, ranging from 20-120 min

The diffractograms of the different CAS-glasses and CMAS-glass can be seen on Figure 5.9 showing an expected broad area for the different CAS and CMAS glasses, indicating an amorphous silica-based network. Hence providing sharper peaks the less silica is in the glass, which corresponds to the amount of silica used for the synthesis of the glasses.

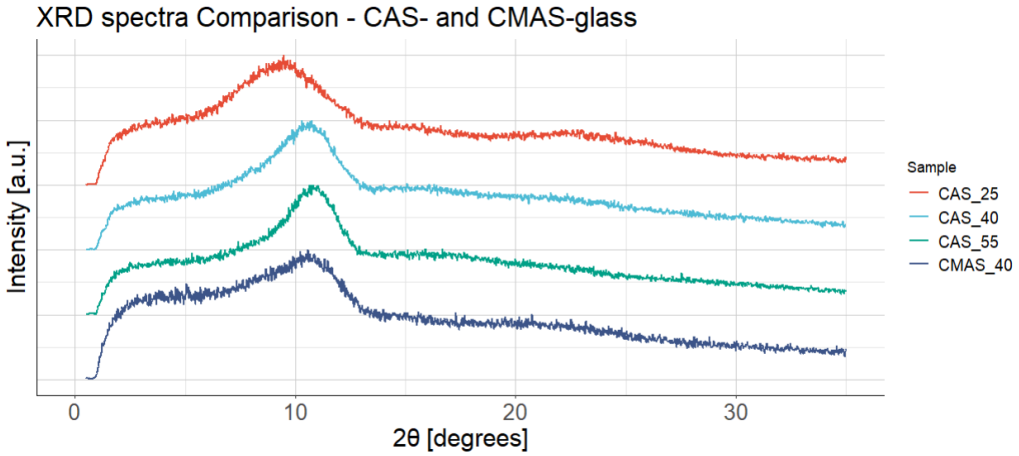

Figure 5.9. Diffractograms of the different CAS- and CMAS-glass

5.0.2 DSC analysis

All the bound water wt% of the different samples ranging from 1, 7, and, 28 days can be observed on Figure 5.10. All of the samples apart from MA Dolomite and $CaCO_3$ have added CH, which reacts with water, which then again is released under the DSC analysis, where the TGA is used to determine how much mass is lost in the specific area that usually lies between 400-500°C. The reason for not adding water to the dolomite and $CaCO_3$, is for the purpose of testing, if CH is released from either material, which would mean a higher reactivity. CH is a product of CaO reaction with water. Hence if any mass loss is observed for these samples, it would mean that the material has released some CaO which under the reactivity test has reacted with water. Showing in Figure 5.10 that no mass loss was observed for $CaCO_3$, which is expected, since thermal decomposition is usually needed, for the release of CO_2. Since $CaCO_3$ did not decompose under the mill times of

60 and 120 min, it is quite interesting to see that dolomite has a mass loss around the designated area, which indicates the formation of CaO. The MA for dolomite also seems to show no sufficient difference between grinding the material for 60 min compared to 120, indicating that maybe a lower amount of mill time can potentially be utilized to yield the same results.

	Bound water (wt%)		
Sample	Day 1	Day 7	Day 28
Kaolin_700(°C)	-0.87	8.59	16.76
Kaolin_800(°C)	-0.03	10.97	18.57
Kaolin_900(°C)	-0.28	10.46	18.35
Ca_MK_700(°C)	0.56	10.18	16.92
Ca_MK_800(°C)	1.89	12.09	16.32
Ca_MK_900(°C)	0.38	11.04	16.21
Kaolin_60min	12	16.09	18.58
Kaolin_120min	4.66	16.07	17.82
Kaolin + Dolomite_60min	11.59	12.02	7.86
Kaolin + Dolomite_120min	9.56	11.03	12.7
Dolomite_60min	5.91	6.31	6.17
Dolomite_120min	6.72	7.34	6.91
Ca_MK_60min	9.96	13.79	12
Ca_MK_120min	12.36	12.91	16.22
CaCO3_60min	----------	----------	----------
CaCO3_120min	----------	----------	----------
CAS_25	3.46	4.32	12.35
CAS_40	3.11	5.11	9.78
CAS_55	1.32	10.53	11.6
CMAS_40	3.11	5.11	9.78

Figure 5.10. Bound water (wt%) of all samples

As shown on Appendix B it can be observed, that not all samples have been measured with the same amount of SCM and CH. This is a product of not enough material being used in the ball mill, since the sample used should be equally activated through MA, resulting in only 1/4 of the jar to be filled, together with the fact, that the samples for the reactivity test have to be sieved to the size between 125-64 µm.

On the bar plot on Figure 5.11 a better visual comparison can be made. The bar plot shows that although kaolin has little to no early reaction when calcined, it shows great early reactivity for the 1 and 7 days MA, with the 28 days being on par with the calcined kaolin and Ca-MK. Where kaolin on its own did not show any activation, a little bit of early activity. The negative or very low values of bound water, can be explained from an apparatus error, where the DSC for all the samples will have its starting mass set to over

100%, which will influence the way, bound water wt% is calculated. which is the difference between the overall mass loss, with that of the designated area around 400-500 °C.

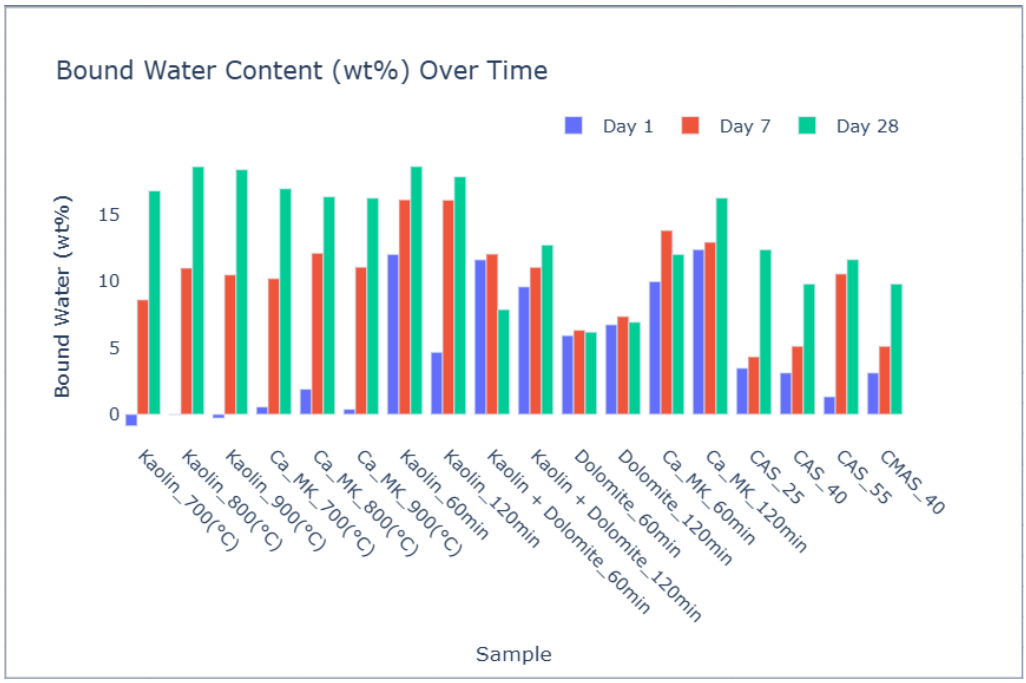

Figure 5.11. Bar plot of bound water (wt%) of all samples

The glass materials show the least amount of reaction, apart from dolomite, where no CH was added. CAS-55 for example, which has the most CaO shows low early reactivity, and a little change between 7 to 28 days, showing that the reaction may stop a couple of days after the 7 day sample. CMAS-40 shows very similar patterns to the CAS-40 glass, whereas CAS-25 has the lowest amount of $CaCO_3$ when synthesizing, but shows the highest bound water wt% after 28 days for the glass materials, but similar early reactivity to CMAS-40 and CAS-40.

On the plot it can also be observed on the abundance of blue bars, that kaolinite contributes to high early reactivity, but when mixed with dolomite the later stage reactivity seems to fall.

5.0.3 Particle size analysis

In this analysis, both the D90 and D50 data are found through a mean value of 3 scans for each sample. The data shows an increase in particle size across the board which can be observed in Figure 5.12. The particle size for all the samples shows to be increasing with the mill time when comparing the D90 values between 20-120 min run times. 120 min shows an increase in the final D90 value across all samples, apart from the Dol + Kao samples which are decreasing gradually with time. This seems counterintuitive since planetary ball mills usually are utilized for grinding the materials to smaller particles. The same pattern has also been observed by Baki, et al. [37], showing a slight increase in particle size of both MA and thermal treatment of kaolin. For MA in a ball mill, with a

mill time of 20 min, the particle size increased from 17.6 µm to 21.7 µm. However, when increasing the mill time to 120 min, it again decreased to 17.6, stating that the layered structure of kaolin could have been delaminated.

When comparing the different materials in size, kaolin which is 60 mol% of the Dol + Kao sample is in the higher end of the particle sizes, with dolomite which is 40 mol% of the mixture, to be in the lower end of particle sizes. The first observation is that both kaolin and dolomite increase in particle size, with the increase of mill time, where a mixture of these show a gradual decrease in size. Furthermore, the values of the Dol + Kao, are closer to the dolomite, than it is to the values of kaolin, which would be expected to be the other way around, since there is more kaolin than dolomite. This could be a product of the materials sticking together when ground, where the particles have not fully dissociated from one another when left for 30 min in a ultrasound-bath, before the analysis was conducted.

The samples of kaolin, Ca-MK, and $CaCO_3$ show a tendency to reach their lowest particle sizes around 80 min of grinding, which then starts to increase at 100 min, and for further increase at 120 min for Ca-MK and $CaCO_3$. Also the values for 80 min run time seem to be closer to each other when comparing all the samples, than the other values that show a wider spread.

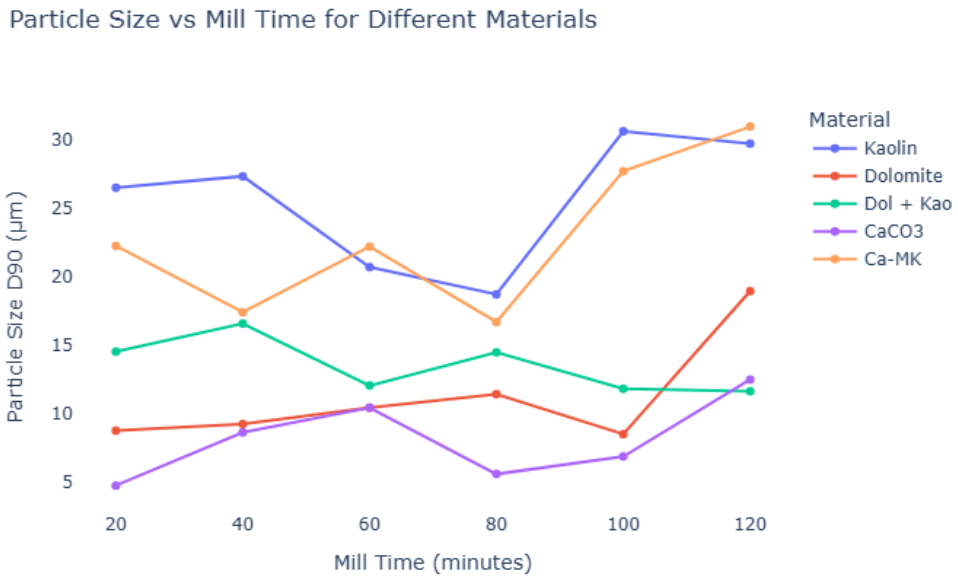

Figure 5.12. Plot of D90 particle size vs mill time for the different materials

.

The box plot on Figure 5.13 was created to enhance visualization and provide a clearer representation of the samples, showing the spread of the particle size. Here the biggest changes are observed for the kaolin and Ca-MK samples, where the rest are closer together. Again here it can be seen, that a mixture of kaolin and dolomite, is much closer to the

particle size of dolomite, than kaolin, also following its low spread. The same goes for kaolin and $CaCO_3$, where the D90 of the mixture lies between the components.

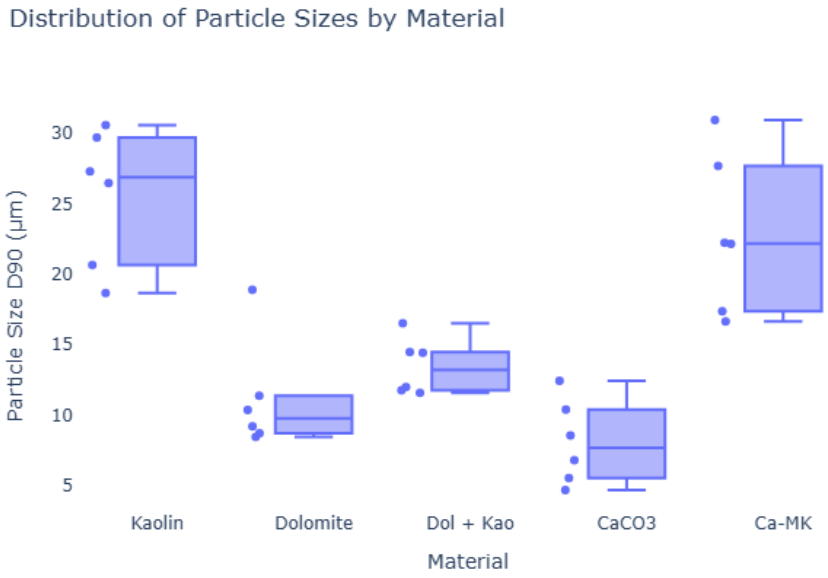

Figure 5.13. Box plot of ball mill samples at the particle size D90

.

5.1 Conclusion

This project, investigates the characteristics of disordered CAS materials, to be used in the cement industry as SCMs, ultimately aiming to find the most optimal and best both economically and environmentally viable material, by comparing the XRD data of the materials, with the bound water in wt%, to analyze which structure of materials have the best pozzolanic reactivity.

The main focus point of materials in this project, is the implementation of kaolin and dolomite, testing both kaolin for thermal treatment on its own and together with the addition of $CaCO_3$ to introduce more Ca to the samples. Besides thermal treatment, MA was also performed on kaolin and Ca-kaolin with the implementation of a planetary ball mill, with different milling times ranging from 20-120 min. Kaolin contributes to high reactivities, under the hydration process. Between the kaolin samples going through thermal and mechanical activation, similar structures have been observed with the help of the XRD, also showing similar results in the reactivity test. Kaolin shows both great early reactivity when ground, but also similar and high bound water values at 7 and 28 days. From both the kaolin and Ca-MK samples, 800 °C seems to be the temperature yielding the highest bound water content. When dolomite is introduced to kaolin, Mg is introduced, showing a significant increase of early reactivity, that without the addition of dolomite was almost non-existent.

The MA of dolomite and $CaCO_3$ show little to no change in crystallinity, but based on the particle size analysis, the particle sizes get bigger with increasing mill times, which also correlates to better reactivity, for the 120 min samples compared to 60 min run time, which is a general trend seen for all the materials that have undergone MA. Dolomite shows the same development of CaO, but with an increase of 100% for the mill time from 60 min to 120 min, shows no significant difference for dolomite, rendering it unnecessary to grind for 2 hours.

Based on the bound water results, both the CAS-glasses and CMAS-glass seem to be in the lower, but at the same time expensive end, rendering it not suitable, if only looking into the pozzolanic reactivity. Both Kaolin and dolomite show great promise as SCMs, with the addition of both Mg and calcium significantly improving early reactivity, especially when looking into MA as a cheaper option than calcine materials at high temperatures.

The DSC can as it has in this project be used to compare the reactivity of different materials. In this project, the focus was the mass loss between 400-500 °C, which corresponds to the amount of CH, making it a relatively fast method to evaluate the pozzolanic reactivity of materials, and how they react compared to each other.

Further work 6

The research presented in this project provides a foundation for understanding the potential of CAS materials, particularly with the addition of kaolin and dolomite blends, as SCMs. However, several key questions remain that need further investigation to get a better understanding of their application in sustainable cement production. This section outlines specific experiments and analyses that could be undertaken to further understand the effects of the materials.

6.1 Optimization of mechanochemical activation

The MA samples in this project were conducted with a small variety of components, with all the samples being ground at 600 RPM in a small ball mill. To optimize the energy used to activate the samples, different RPM and run times, together with more compositions could be interesting to investigate, now that for the bound water test, MA shows almost as great promise as calcination. Parameters such as optimal sample weight and ball/powder ratios could have an impact on the outcome also.

6.1.1 Refinement and Validation of DSC-Based Reactivity Test

The DSC method for assessing pozzolanic reactivity shows promise as a rapid and convenient technique. However, the issues with the DSC in this project, needs to be addressed since the values of mass loss should never be negative, showing an increase of mass, when heated to 580 °C. This introduces an error source, rendering the data for the samples being less reliable, when comparing with other studies.

In regards to the reactivity test, only 1, 7, and 28 days of hydration were conducted in this project. With more frequent sampling and longer hydration times, more precise and reliable data will be obtained.

6.1.2 Microstructural Characterization

To gain a deeper understanding of the mechanisms by which MA-treated kaolin and dolomite enhance cement hydration, microstructural analysis is essential. Analysis methods to get a better understanding involve:

- Scanning Electron Microscopy: can be used to image the morphology and particle size distribution of the raw, calcined and MA-treated SCMs. In hydrated cement

pastes, SEM can be used to observe and compare the changes under the treatment of materials.

- Transmission Electron Microscopy: can be used to investigate the nanoscale structure of the materials and the interaction between the SCMs and the cement matrix.
- X-ray Photoelectron Spectroscopy: this technique can provide information on the chemical composition and oxidation states of elements at the surface of the materials.

6.1.3 Performance Evaluation in Mortar and Concrete

While reactivity tests provide valuable insights, the ultimate assessment of SCM performance lies in evaluating the properties of mortar and concrete mixtures. Which together with the other points could give insight to the properties of the final products

Compressive Strength Testing: Mortar mixtures incorporating varying proportions of the SCMs rendered interesting in this project can be prepared and tested for compressive strength at different ages, which could be 1, 7, 28, 56, and 90 days).

Bibliography

[1] Chatbot App - AI Chatbot — chat.chatbotapp.ai. `https://chat.chatbotapp.ai`. [Accessed 06-05-2025].

[2] davidrguez. Portland Cement Types — thecementinstitute.com. `https://thecementinstitute.com/portland-cement-types/`. [Accessed 03-12-2024].

[3] Where is cement used? - Cembureau — lowcarboneconomy.cembureau.eu. `https://lowcarboneconomy.cembureau.eu/where-is-cement-used/`. [Accessed 03-12-2024].

[4] The story of cement manufacture - Cembureau — lowcarboneconomy.cembureau.eu. `https://lowcarboneconomy.cembureau.eu/the-story-of-cement-manufacture/`. [Accessed 03-12-2024].

[5] Zbigniew Giergiczny. Fly ash and slag. *Cement and Concrete Research*, 124, October 2019.

[6] Gabriel Varga. The structure of kaolinite and metakaolinite. *Epitoanyag - Journal of Silicate Based and Composite Materials*, 59(1):6–9, 2007.

[7] Ishrat Baki Borno and Warda Ashraf. Effects of co-calcining kaolinite-rich clay blends with alkali and alkali earth metal hydroxides. *Applied Clay Science*, 231, January 2023.

[8] Harris ApS. Om ler og farver, 2023. https://www.harris.dk/knowledge/om-ler-og-farver. Last accessed 15 January 2025.

[9] F. Bergaya and G. Lagaly. *Chapter 1 General Introduction: Clays, Clay Minerals, and Clay Science*, page 1–18. Elsevier, 2006.

[10] Neeraj Kumari and Chandra Mohan. Basics of clay minerals and their characteristic properties. In Gustavo Morari Do Nascimento, editor, *Clay and Clay Minerals*, chapter 2. IntechOpen, Rijeka, 2021. doi: 10.5772/intechopen.97672.

[11] Esperanza Pavón and María D. Alba. Swelling layered minerals applications: A solid state nmr overview. *Progress in Nuclear Magnetic Resonance Spectroscopy*, 124-125:99–128, 2021. doi: https://doi.org/10.1016/j.pnmrs.2021.04.001. Last accessed 12. December 2023.

[12] Esperanza Pavón and María D. Alba. Swelling layered minerals applications: A solid state nmr overview. *Progress in Nuclear Magnetic Resonance Spectroscopy*, 124–125:99–128, 2021. doi: 10.1016/j.pnmrs.2021.04.001.

[13] Linda Bloomfield. clay structure. *Ceramics Monthly*, 2016. https://lindabloomfield.co.uk/wp-content/uploads/2016/06/Bloomfield_June16.pdf. Last accessed 18 December 2024.

[14] G. Brown, P. Nadeau, Leslie Fowden, Richard Maling Barrer, and P. B. Tinker. Crystal structures of clay minerals and related phyllosilicates. *Philosophical Transactions of the Royal Society of London. Series A, Mathematical and Physical Sciences*, 311(1517):221–240, 1984. doi: 10.1098/rsta.1984.0025. Last accessed 12. December 2023.

[15] OpenLearn. An introduction to minerals and rocks under the microscope. https://shorturl.at/flrHT. Last accessed 28 September 2023.

[16] Alfonso Hernández-Laguna, Elizabeth Escamilla-Roa, Vicente Timón, Martin T. Dove, and C. Ignacio Sainz-Díaz. Dft study of the cation arrangements in the octahedral and tetrahedral sheets of dioctahedral 2:1 phyllosilicates. *Physics and Chemistry of Minerals*, 33:655–666, 2006. doi: 10.1007/s00269-006-0120-z. Last accessed 13. December 2023.

[17] Steven Earle. Silicate minerals. In *Psysical Geology*, chapter 2.4. BCcampus, 2019. `https://opentextbc.ca/geology/chapter/2-4-silicate-minerals/`.

[18] Cornelis Klein. Nesosilicates. Unknown. `https://www.britannica.com/science/mineral-chemical-compound/Nesosilicates`. Last accessed 28 September 2024.

[19] Matvei Zinkevich. Thermodynamics of rare earth sesquioxides. *Progress in Materials Science*, 52(4):597–647, 2007. doi: https://doi.org/10.1016/j.pmatsci.2006.09.002. Last accessed 6. December 2023.

[20] Gersten Smith. *The Physics and Chemistry of materials*. Wiley Interscience, 2001.

[21] University of Waikato Science Learning Hub – Pokapū Akoranga Pūtaiao. Carbonate chemistry, 2012. `https://www.sciencelearn.org.nz/resources/469-carbonate-chemistry`. Last accessed 06. December 2023.

[22] LibreTexts. Glass formers and network modifiers, Unknown. `https://shorturl.at/gwKM9.Lastaccessed10`. Last accessed 06 December 2023.

[23] C. Huang and E.C. Behrman. Structure and properties of calcium aluminosilicate glasses. *Journal of Non-Crystalline Solids*, 128(3):310–321, May 1991.

[24] M. Ozabaci, M.A. Aksan, G. Kirat, O. Kizilaslan, and M.E. Yakinci. Preparation and characterization of cao-al 2 o 3 -sio 2 (cas) glass-ceramics. *Journal of Non-Crystalline Solids*, 454:8–12, December 2016.

[25] M. Turchi, S. Perera, S. Ramsheh, A.. Popel, D.V. Okhrimenko, S.L.S. Stipp, M. Solvang, M.P. Andersson, and T.R. Walsh. Predicted structures of calcium aluminosilicate glass as a model for stone wool fiber: effects of composition and interatomic potential. *Journal of Non-Crystalline Solids*, 567:120924, September 2021.

[26] Mette Moesgaard, Duncan Herfort, Mette Steenberg, Lise Frank Kirkegaard, and Yuanzheng Yue. Physical performances of blended cements containing calcium aluminosilicate glass powder and limestone. *Cement and Concrete Research*, 41(3):359–364, March 2011.

[27] H F W Taylor. *Cement chemistry, second edition.* Thomas Telford, London, England, 2 edition, January 1997.

[28] Britannica. Cement - Extraction, Processing, Manufacturing | Britannica — britannica.com. `https://www.britannica.com/technology/cement-building-material/Extraction-and-processing`. [Accessed 31-03-2025].

[29] H F W Taylor. *Cement chemistry, second edition.* Thomas Telford, London, England, 2 edition, January 1997.

[30] Nicholas B winther. Bogue calculation — understanding-cement.com. `https://www.understanding-cement.com/bogue.html`. [Accessed 31-03-2025].

[31] Seham S. Alterary and Narguess H. Marei. Fly ash properties, characterization, and applications: A review. *Journal of King Saud University - Science*, 33(6):101536, September 2021.

[32] B.K. Shahraki, B. Mehrabi, and R. Dabiri. Thermal behavior of zefreh dolomite mine (central iran). *Journal of Mining and Metallurgy, Section B: Metallurgy*, 45(1):35–44, 2009.

[33] Cargohandbook. Dolomite - cargo handbook - the world's largest cargo transport guidelines website — cargohandbook.com. `https://cargohandbook.com/Dolomite`. [Accessed 08-05-2025].

[34] Éva Makó. The effect of quartz content on the mechanical activation of dolomite. *Journal of the European Ceramic Society*, 27(2–3):535–540, jan 2007.

[35] Miłosz Szybilski and Wiesława Nocuń-Wczelik. The effect of dolomite additive on cement hydration. *Procedia Engineering*, 108:193–198, 2015.

[36] P.G Caceres and E.K Attiogbe. Thermal decomposition of dolomite and the extraction of its constituents. *Minerals Engineering*, 10(10):1165–1176, 1997.

[37] Vahiddin Alperen Baki, Xinyuan Ke, Andrew Heath, Juliana Calabria-Holley, Cemalettin Terzi, and Murat Sirin. The impact of mechanochemical activation on the physicochemical properties and pozzolanic reactivity of kaolinite, muscovite and montmorillonite. *Cement and Concrete Research*, 162, December 2022.

[38] Stephen E. Kaczmarek, Jay M. Gregg, David L. Bish, Hans G. Machel, and Bruce W. Fouke. *Dolomite, very High-magnesium calcite, and microbes-implications for the microbial model og dolomitization.* SEPM (Society for Sedimentary Geology), 2017.

Ball Mill samples A

CaCO3 (5g)	Time(min)
1.	20
2.	40
3.	60
4.	80
5.	100
6.	120

Dolomite + kaolinite (3g)	Time(min)
1.	20
2.	40
3.	60
4.	80
5.	100
6.	120

Dolomite (3g)	Time(min)
1.	20
2.	40
3.	60
4.	80
5.	100
6.	120

Ca-MK (3g)	Time(min)
1.	20
2.	40
3.	60
4.	80
5.	100
6.	120

Figure A.1. Measured values and run time for the mechanochemical activation

Measured values of SCM and CH

B

In this appendix, the amount of SCM and portlandite, measured for the reactivity test is shown.

Measured amount of SCM and Portlandite		
Sample	SCM (g)	Portlandite(g)
Kaolin_700(°C)	0,9955	3,0185
Kaolin_800(°C)	1,0022	3,0016
Kaolin_900(°C)	1,0054	3,0019
Ca_MK_700(°C)	1,0098	3,0005
Ca_MK_800(°C)	1,0061	3,0128
Ca_MK_900(°C)	1,0069	3,0011
Kaolin_60min	0,9921	3,0284
Kaolin_120min	0,5006	1,5054
Kaolin + Dolomite_60min	0,9998	3,0019
Kaolin + Dolomite_120min	0,9988	2,974
Dolomite_60min	0,9997	0
Dolomite_120min	0,9013	0
Ca_MK_60min	1,0015	3,0107
Ca_MK_120min	0,9997	2,9996
CaCO3_60min	0,8029	0
CaCO3_120min	1,0013	0
CAS_25	1,0063	2,996
CAS_40	1,0018	3,026
CAS_55	0,9987	3,0429
CMAS_40	1,0001	2,9974

Figure B.1. Measured values of SCM and Portlandite in grams

Measured values of samples for DSC C

Weighed amount of sample for DSC analysis (mg)			
Sample	Day 1	Day 7	Day 28
Kaolin_700(°C)	26,8	19,4	18,7
Kaolin_800(°C)	22,9	18,4	20,3
Kaolin_900(°C)	21,9	18,9	23,9
Ca_MK_700(°C)	26,9	18,7	15,9
Ca_MK_800(°C)	23,3	19,1	17,8
Ca_MK_900(°C)	19,8	17,5	17,2
Kaolin_60min	19,4	19,3	19,3
Kaolin_120min	18,4	15,1	21,8
Kaolin + Dolomite_60min	20,9	17,2	15,3
Kaolin + Dolomite_120min	18,4	17,3	16,3
Dolomite_60min	22,4	23,6	30,8
Dolomite_120min	22,6	29,8	27
Ca_MK_60min	18,7	17,2	20,1
Ca_MK_120min	17,3	18,2	17,4
CaCO3_60min	21,4	20,2	19,9
CaCO3_120min	25,7	26,1	29,3
CAS_25	23	23,6	18,7
CAS_40	25,8	19,7	21
CAS_55	19	23,7	19,1
CMAS_40	17,6	21,4	9,78

Figure C.1. Measured values of sample for DSC analysis

Excel - purity calculation of Kaolin and Dolomite

D

The data used in the Excel sheet, is obtained from a DSC analysis, heating the samples to 950 °C, and calculating the weight loss observed, which is then compared to the theoretical weight loss for the evaporation of $2\,H_2O$ for kaolin, and $2\,CO_2$ for the dolomite sample.

	Kaolinite	When calcinated the kaolinite loses 2H2O, and becomes Metakaolin								
	Theoretical purity (fraction):	0,86043322								
		Through the mass loss observed (DSC)								
		Instead of taking the final value/values of mass loss, here we look at the bend in the curve this indicates kaolinite releasing water								
	Observed purity %	84,94312	%							
	Observed purity (fraction):	0,8494312								
		But the sample still loses mass afterwards wich is an indication of an impurity. Here the mean value of the last 2 data points is used								
		84,51797	%							
		84,51953	%							
	avg.	84,51875	%							
Absolute mass loss (Fraction)		0,8451875								
	Purity of kaolinite:		Observed mass loss/theoretical mass loss=					0,982281	fraction	
	Absolute purity:		Observed mass loss/theoretical mass loss=							
	The purity of kaolinite is therefore			98,22813446	%					
	this indicates impurity of			1,771865539	%					
	Further confirmation through XRD is needed, to find the impurity of the kaolinite									
	Dolomite	Ignore the dolomite so far								
	Around 755 and 815 Deg C Dolomite loses 2CO2, and we get MgO and CaO									
	Weight after calcination (%) DSC:		53,7748	%			0,537748	fraction		
	Theoretical weight (%):		52,26778742	%			0,5227	fraction		
	Purity(%) = Actual weight loss/theoretical:		1,028832531							
	Even though it is theoretically improbable, i am asuming 100% purity									
	MgO+CaO	96,3818	g/mol	At this step, we asume 1:1 ratio						

Figure D.1. Excel - Calculations of the purity of Kaolin and Dolomite used in this project

Diffractograms of pure $CaCO_3$ (A) and Dolomite (B)

E

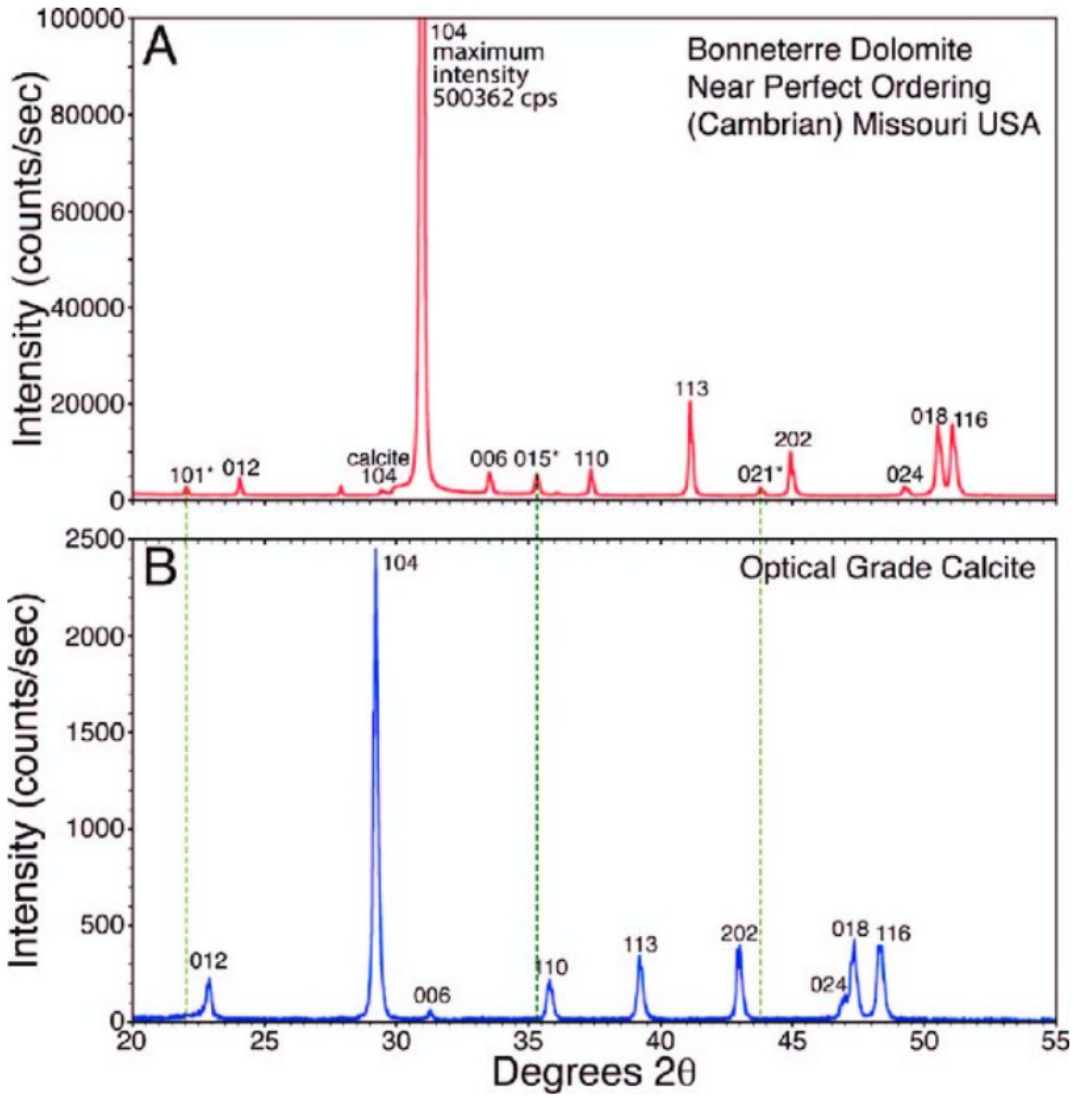

Figure E.1. Diffractogram of $CaCO_3$ and dolomite, Edited from [38]

Raw particle size data F

In this appendix, the gathered data for both D90 and D50 are presented. Where the values for both D90 and D50 are given in µm, and represent what % of the samples are at that given value, or smaller. This means that at D90 for sample 1 of kaolin, 90% of the particles have a diameter of 26.45 µm or below, as for the same sample the particle size at D50 is 5.873

Particle_Size_Data_D90			
Material	**Sample**	**Mill Time (min)**	**Particle Size(D90)**
Kaolin	1	20	26.45
Kaolin	2	40	27.29
Kaolin	3	60	20.65
Kaolin	4	80	18.67
Kaolin	5	100	30.57
Kaolin	6	120	29.67
Dolomite	1	20	8.726
Dolomite	2	40	9.205
Dolomite	3	60	10.38
Dolomite	4	80	11.37
Dolomite	5	100	8.456
Dolomite	6	120	18.9
Dol + Kao	1	20	14.49
Dol + Kao	2	40	16.52
Dol + Kao	3	60	12
Dol + Kao	4	80	14.43
Dol + Kao	5	100	11.77
Dol + Kao	6	120	11.59
CaCO3	1	20	4.708
CaCO3	2	40	8.573
CaCO3	3	60	10.39
CaCO3	4	80	5.537
CaCO3	5	100	6.818
CaCO3	6	120	12.44
Ca-MK	1	20	22.21
Ca-MK	2	40	17.37
Ca-MK	3	60	22.15
Ca-MK	4	80	16.65
Ca-MK	5	100	27.66
Ca-MK	6	120	30.91

Figure F.1. D90 values for particle size analysis of all ball mill samples given in µm.

Particle_Size_Data_D50			
Material	**Sample**	**Mill Time (min)**	**Particle Size(D50)**
Kaolin	1	20	5.873
Kaolin	2	40	5.967
Kaolin	3	60	4.807
Kaolin	4	80	4.543
Kaolin	5	100	4.48
Kaolin	6	120	5.176
Dolomite	1	20	4.144
Dolomite	2	40	3.343
Dolomite	3	60	4.392
Dolomite	4	80	4.128
Dolomite	5	100	3.817
Dolomite	6	120	5.802
Dol + Kao	1	20	6.041
Dol + Kao	2	40	5.05
Dol + Kao	3	60	4.903
Dol + Kao	4	80	4.797
Dol + Kao	5	100	4.817
Dol + Kao	6	120	4.948
CaCO3	1	20	1.483
CaCO3	2	40	2.473
CaCO3	3	60	3.341
CaCO3	4	80	1.943
CaCO3	5	100	2.442
CaCO3	6	120	3.618
Ca-MK	1	20	5.705
Ca-MK	2	40	5.349
Ca-MK	3	60	5.267
Ca-MK	4	80	4.599
Ca-MK	5	100	4.943
Ca-MK	6	120	6.477

Figure F.2. D50 values for particle size analysis of all ball mill samples given in µm.